NASA Technical Memorandum 86384

Vapor-Screen Technique for Flow Visualization in the Langley Unitary Plan Wind Tunnel

Odell A. Morris, William A. Corlett,
Donald L. Wassum, and C. Donald Babb
Langley Research Center
Hampton, Virginia

NASA
National Aeronautics
and Space Administration
Scientific and Technical
Information Branch
1985

SUMMARY

The vapor-screen technique for flow visualization in the Langley Unitary Plan Wind Tunnel (UPWT) is presented with a description of the light sources and photographic equipment used. The tests were conducted with a variation in lighting, camera setting, and vapor densities to determine the conditions required in the UPWT to obtain high-quality vapor-screen photographs. Mach number was varied from 1.47 to 4.63 at angles of attack up to 35°.

Typical vapor-screen photographs of various flow patterns are presented to illustrate both the quality of the photographs and how they are used in flow analysis. The use of the vapor-screen technique in the UPWT is a valuable tool for flow visualization in the supersonic speed range. Accurate measurements of shocks and vortex locations have been obtained, and direct comparison with theoretical calculations of the shock and vortex patterns is possible.

INTRODUCTION

The vapor-screen technique of flow visualization has served as a valuable diagnostic tool in the study of flow fields at supersonic speeds for three decades (refs. 1 to 3). Recognition of the merits of this technique has led to numerous refinements in an effort to obtain higher quality vapor-screen photographs. Because the vapor-screen technique is particularly useful in the study of complex flow fields, such as those of missiles at high angle of attack and wing leading-edge vortices at supersonic speeds, improvements in the vapor-screen technique were undertaken in the Langley Unitary Plan Wind Tunnel (UPWT). Vapor-screen photographs obtained during this development stage are presented in references 4 to 8.

Vapor-screen experiments are conducted in the UPWT in a manner similar to that used for other wind-tunnel tests except that a controlled amount of water is added to the tunnel flow. This water condenses (and possibly freezes into ice crystals) to form a thin, uniformly distributed fog. This fog is then illuminated by a narrow sheet of light that is projected through the tunnel perpendicular to the free-stream flow. The presence of the model in the flow field alters the uniform distribution of fog and, consequently, the degree of illumination. The results are distinct flow patterns that are visible on the illuminated fog sheet. This sheet of illuminated fog or condensate is commonly referred to as a "vapor" screen, although vapor would not be visible; nevertheless, this misnomer will be continued in this paper.

The purpose of the present paper is to provide a description of the vapor-screen technique as developed for use in the UPWT and to present typical vapor-screen photographs for various test conditions and system parameters. Several examples are presented in which vapor-screen results have contributed to the understanding of complex flow fields and have provided a basis for theoretical calculations.

SYMBOLS

C_p	pressure coefficient
l	model reference body length, in.
M	free-stream Mach number
p_t	tunnel stagnation pressure, atm
R	Reynolds number per foot
T	temperature, °F
$T_{dp,atm}$	dew point corrected to standard atmospheric pressure, °F
$T_{dp,\infty}$	dew point corrected to free-stream static pressure, °F
T_t	stagnation temperature, °F
T_∞	test-section static temperature, °F
t	camera exposure time, sec
x	longitudinal station measured from model nose, in.
α	angle of attack, deg
η	fraction of local wing semispan
Λ_{LE}	leading-edge sweep angle, deg
ϕ	model roll angle, deg

APPARATUS AND PROCEDURE

Facility

The vapor-screen tests were conducted in the Langley Unitary Plan Wind Tunnel (UPWT) in both test section 1 with a Mach number range from 1.47 to 2.86 and test section 2 with a Mach number range from 2.30 to 4.63. A schematic drawing of the facility is shown in figure 1. This tunnel, which is a continuous-flow facility with two 4-ft by 4-ft by 7-ft test sections, is described in reference 9. The vapor-screen test technique is similar to those developed previously in the former Langley 4-Foot Supersonic Pressure Tunnel (ref. 2) and in other facilities.

General Test Procedure

A sketch of the apparatus used in the UPWT vapor-screen setup is shown in figure 2(a). The high-intensity light source is mounted outside the test section and positioned to project a sheet of light perpendicular to the tunnel flow. Cameras may be positioned outside the tunnel and/or mounted inside the test section to photograph the vapor-screen flow pattern from either position (fig. 2(b)). Details of the

1000-W mercury-vapor lamp assembly are provided in figure 2(c). Photographs showing the inside camera and typical models ready for tests in both the low Mach number test section and the high Mach number test section are presented as figures 3(a) and 3(b), respectively.

The model to be tested is painted with a flat black paint to reduce the glare from the lights, and reference marks are painted on the model at stations where photographs are to be taken. Prior to the test, the cameras are set up and focused by using a target located at the axial position of the light screen. For a typical test, water is injected into the tunnel downstream of the test section (see fig. 1) to produce the required fog density.

The main sting support system in the tunnel, which provides angle-of-attack variation, also allows the model to be rolled and positioned longitudinally. After the vapor screen has been established, the model is positioned at various locations relative to the vapor screen by movement of the model longitudinally, in angle of attack, or in roll by using the sting support system. This procedure thus allows photographs to be made along the entire length of the model through a wide range of angle of attack and roll so that an overall view of the flow pattern may be obtained without changing the position of the camera relative to the lights.

Photographic Equipment

The photographic equipment used in the current vapor-screen system at the UPWT is a remote-controlled 70-mm single-lens reflex camera with an 80-mm f/2.8 planar lens. A battery-operated motor, which is an integral part of the camera, automatically advances the film and cocks the shutter. The camera magazine is designed to take up to 15 ft of cassette-loaded 70-mm film, which provides for about 70 photographs per roll. An ASA 400 film is normally used.

The camera located inside the tunnel (fig. 2(b)) is housed in a metal box with a plate-glass window 0.25 in. thick to protect the camera lens. The unit is supported from the top of the tunnel by a 2-in-diameter metal tube. In the early stages of the development of the system it was discovered that temperature increases inside the box could cause camera malfunctions. These problems were alleviated when moisture-controlled cooling air was injected into the housing to prevent the camera from overheating. A remote-control exposure device was designed and built for use on the inside tunnel camera that allowed exposure time settings from 1/15 to 1 sec. In addition, a small red indicator light was built into the camera remote-control timer to confirm successful shutter operation. This feature allows the operator to abort tunnel runs at the first signal of camera failure, thereby saving considerable tunnel operation time. The camera located outside the tunnel is mounted on a test-section window support bar and uses a mirror to obtain a wider field of view through the test-section window bars (fig. 2(b)).

A series of tests were conducted with different camera exposure times and aperture settings. Vapor-screen photographs will be shown and discussed subsequently that indicate which times and settings produced the best results.

Light-Source System

In order to produce a good vapor-screen photograph, the light source must provide an intense beam of light with a very narrow width. This sheet of light should

be well-defined with sharp edges and very little stray light. To provide these characteristics, the light source used for most of these tests consisted of two 1000-W mercury-vapor lamp assemblies and their related power supplies. Each 5- by 10-in. metal box encases a bulb and an adjustable 1.5-in-diameter parallax cylindrical lens and knife edge (fig. 2(c)). The knife edges are located just forward of the bulb in each assembly and can be adjusted to vary the intensity of the light emitted from the bulb. In combination with the adjustable parallax lens, a vertical light screen of proper intensity and width (1/4 in.) can be obtained.

In addition to the tests with the mercury-vapor lamp setup, a few tests were made by using a 15-mW helium-neon laser light source and a 4-W argon-ion variable-power laser. The laser projected a light beam 0.125 in. in diameter and was fanned out across the tunnel with a 0.15-in-diameter glass rod mounted in front of the laser beam.

Water-Injection System

To establish a "vapor" screen for photography, the water injected into the tunnel must be carefully controlled to provide a fog density sufficient to scatter the light without being too dense to diffuse the scattered light. Control of the moisture within the tunnel circuit is maintained with the dry-air inbleed and outbleed system (described in ref. 9) in conjunction with a water-injection system. The water-injection system consists of a single orifice in the top wall of the diffuser section of each test section. For all tunnel operating conditions, the static pressure inside the tunnel at the water-injection station is well below atmospheric pressure. The water is, therefore, injected in controlled amounts by a valve in the waterline connected to an external reservoir. Depending on the existing moisture in the tunnel circuit and test conditions, a nominal run requires about 3 to 5 qt of water to provide a vapor screen. Once the required dew point is obtained, water does not have to be added again for several minutes. The condensate is vaporized in the tunnel circuit and recondensed in the supersonic nozzle.

The mixture of air and water vapor is continuously sampled at the quiescent chamber for each test section, and a dew-point instrument is used to monitor the fog density. Although measurements are made at tunnel stagnation conditions, all dew-point values are corrected to standard atmospheric pressures.

Tunnel Conditions for Optimum Screen

Tunnel flow conditions for vapor-screen photographs over the Mach number range of both test sections of the UPWT are presented in figure 4. Test variables are presented at stagnation conditions, with the exception of dew-point values that have been corrected to standard atmospheric conditions. The moisture content corresponding to the range of dew-point values shown in figure 4 varies from 2000 to 8000 parts per million. It is significant to note that for the lower Mach numbers, the tunnel stagnation temperature is well below the standard operating value of 125°F for the UPWT. (The standard operating temperature is 150°F for Mach numbers above 3.8.) In fact, vapor screens at a Mach number of 1.5 cannot always be obtained because of the required low tunnel operating temperature that often exceeds the limit of the cooling tower of the tunnel on hot, humid days.

DISCUSSION OF RESULTS

An analysis of the lower operating boundary for acceptable fog density for good vapor-screen photographs has been made and the results are presented in figure 5. Water is added downstream of the test section (see fig. 1) and is fully vaporized in the circuit of the continuous-flow facility. The airstream is cooled during acceleration in the nozzle to supersonic speeds; however, it has been determined that a large amount of supersaturation is required for condensation. Hence, the airstream must be cooled well below the saturation temperature for condensation to occur in the supersonic nozzle. For these conditions, condensation will occur suddenly and the large amount of heat added to the air during the condensation process will cause condensation shocks.

Supercooling increments of about 80°F have been measured in several small tunnels (ref. 10). For larger tunnels with long test sections, reference 10 suggests that a conservative supercooling increment would be 54°F. This value was verified in the UPWT by raising tunnel stagnation temperature to the condition at which the vapor-screen condensate was no longer visible. The screen typically disappeared as test-section static temperatures approached a value approximately 54°F below computed saturation temperatures. The test-section static temperature T_∞ plus the supercooling increment of 54°F (that is, T_∞ + 54°F) has been plotted to show the lower condensation boundaries at tunnel stagnation temperatures T_t of 95°F and 125°F (fig. 5). To the right of these curves, sufficient supercooling is available to condense water vapor from the airstream. Also shown in figure 5 are measured dew points adjusted to free-stream static pressure that provide optimum vapor screens for the UPWT. For greater values of $T_{dp,\infty}$, the fog is too dense; and for lower values of $T_{dp,\infty}$, the fog is too thin. As shown in figure 5, the minimum test Mach number for obtaining optimum vapor screens at the standard operating temperature, T_t = 125°F, is approximately 1.7. At the UPWT low operating limit of T_t = 95°F, optimum vapor screens can be obtained at M = 1.5.

Water-vapor condensation obviously affects the free-stream condition in the test section. This raises the question of the validity of comparing vapor-screen results with other data, such as force and moment data obtained at dry tunnel conditions.

Condensation at supersonic speeds is accompanied by a stagnation-pressure loss and a decrease in Mach number at the condensation shock. Orders of magnitude of these effects are presented in references 9 and 10. At Mach 2.0, for example, it is estimated that stagnation pressure is reduced 5 percent, Mach number is reduced by 0.05, and static pressure is increased by 4 percent. However, it is felt that errors of this magnitude will not affect the interpretation of vapor-screen photographs. Typical measurements of normal-force coefficients obtained at dry tunnel conditions vary about 5 percent when compared with force data obtained during vapor-screen tests. Therefore, valid forces and moments cannot be obtained during a vapor-screen test; a duplicate test is required at dry tunnel conditions.

Effect of Light-Source Location and Camera Settings

The effect of light-source location with respect to the camera was tested and is shown in a series of photographs (fig. 6). A comparison of the photographs indicates that no large differences in photograph quality were obtained because of light-source location when using the 1000-W mercury light source. However, the photographs taken with the single light mounted on the same side as the camera (fig. 6(a)) provide a more desirable vapor-screen picture because this technique eliminates the dark shadow

cast by the single light source when the camera is mounted on the opposite side of the tunnel (fig. 6(b)). The photographs of figure 6(c) may have a slightly improved image detail because of the increase in light intensity, but the shadow effect is only partially eliminated by the addition of the second light (one light on each side of the tunnel). The alignment and setup time of the two lights on opposite sides of the tunnel were found to be more time-consuming. Tests with both lights mounted as a unit on the same side of the tunnel gave good overall results and required minimum setup time for regular day-to-day operation.

During tests with the 15-mW helium-neon laser light source, very sharp images on the vapor screen were obtained; but the camera exposure time had to be increased to about 4 sec (fig. 7). Because of model dynamics, the long exposure time resulted in a blurring of the vapor-screen image. In an effort to increase the light level, tests were conducted by using a larger 4-W argon-ion (Ar^+) variable-power laser. Photographs obtained at $M = 4.5$ using the more powerful laser are shown in figure 8. Camera exposure time required for these photographs was considerably less, 1/8 to 1/2 sec, and the detail appears better than in the photographs obtained with either the small laser or the 1000-W mercury vapor lamps. Additional tests using the large laser light have been planned to evaluate its potential more fully; any advantages must be weighed, however, against the increased cost and its very restrictive operation because of its large size and the elaborate safety precautions required.

A camera exposure time of 1/4 sec and an f/2.8 aperture setting, along with two 1000-W mercury-vapor light sources mounted on the same side of the tunnel as the camera, were selected as the optimum setup for the vapor-screen photographs presented in this paper.

Effect of Varying Fog Density

Examples of the effect of fog density on the vapor-screen photographs are shown in figure 9 at $M = 2.35$ and $R = 2.0 \times 10^6$ per foot. At tunnel dew points from 5°F to 15°F, the flow field is barely visible when viewed by eye and does not produce adequate illumination for good photographs. The photographs show that the best dew point at $M = 2.35$ is between 25°F and 30°F. As the dew point approached 45°F, the fog density was so thick that the portion of the model on the camera side of the vapor screen was blurred.

Effect of Reynolds Number

As seen in the vapor-screen photographs, variation of tunnel Reynolds number at $M = 2.35$ (fig. 10) shows an effect similar to the dew-point effect discussed previously (fig. 9). That is, increasing the Reynolds number from 1.0×10^6 to 4.5×10^6 per foot by varying the pressure (while maintaining a constant dew point of 30°F) appears to increase the fog density to the point at which the model at the high Reynolds number is barely visible. Further tests indicated that the optimum vapor screen in the higher Reynolds number range (about 4.0×10^6 to 4.5×10^6 per foot) required a reduction in the dew point to about 15°F to 20°F. The trends shown are representative of the test range of Mach numbers.

Application and Analysis

The information provided by vapor-screen photographs, although qualitative in nature, can be used to analyze complex flow fields. Three types of phenomena are defined by the vapor-screen technique. The first type is the change in flow density through oblique shock waves. This change results in a similar change in fog density that, when illuminated, provides a clear definition of the shock position and shape. The second type involves a flow phenomenon resulting from boundary-layer separation such as wakes, vortex feed sheets, and vortex cores. Apparently, during the process of flow separation, particles are not convected across the shear line into the wake flow. As a result, the absence of particles to illuminate will cause wakes, feed sheets, and vortex cores to appear dark or transparent. A third type of phenomenon involves a phase change of the visible condensate (or ice crystals) to the transparent gaseous state (vapor) in a flow region where large temperature gradients are present.

Illustrated in figure 11 are examples of the first two types of flow phenomena that are typical of most vapor-screen photographs. The bow shock is clearly visible as indicated by the different intensity levels. The vortex feed sheets and vortex cores formed by flow separation on the sides of the body appear either as transparent areas or as dark areas without particles present to reflect the light.

Vapor-screen photographs are often difficult to interpret because they show a two-dimensional view of the flow field with a three-dimensional view of the model exposed beyond the vapor screen. Also, the dark shadows cast by the model from the light source sometimes appear as part of the model, which may add to the confusion (fig. 11).

To obtain an overall view of the shock-wave/vortex-wake pattern, a series of photographs can be taken along the length of the model. These can be obtained with either the inside or outside camera setup, with each method having certain advantages. For example, a series of photographs taken with the outside camera provide a perspective view of the overall flow field, as shown in the photographs of figure 12(a). By properly choosing the light and camera position, the shadow can be eliminated. A similar composite display can be obtained from photographs taken with the inside camera; however, the view is more restricted to the flow pattern as seen from the rear of the model (fig. 12(b)). Photographs obtained by using the inside camera show a flow pattern in a plane normal to the free-stream flow, and therefore more accurate measurements of the shock and vortex locations can be obtained.

Examples of photographs taken with the inside camera, as shown in figure 13, are rear views of a typical cruciform missile model at various stations for α = 11.5°, 23.2°, and 35.2°. The photographs of figures 14(a) and 14(b) show typical vapor-screen photographs obtained on a fighter-type airplane configuration at various stations for α = 3° and 10°, respectively.

Vapor-screen photographs are used for a direct comparison with theoretical calculations of the shock displacement and vortex patterns. The use of vapor-screen photographs to evaluate theory is shown in figure 15. Analytical methods were developed and reported in reference 11 to predict the strength and position of the vortices on cylindrical missiles with wing and tail fins. Figure 15 shows a comparison of the theoretical vortex position and size with vapor-screen photographs taken in a

plane at the aft end of the missile at various roll angles. The existence of the vapor-screen data in this case provided a qualitative means of evaluating the vortex-tracking theory and resulted in a high degree of confidence in the accuracy of the overall analysis of reference 11.

The high-quality resolution available in the vapor-screen photographs obtained in the UPWT has made possible a detailed analysis of complicated leeside wake flows. Reference 12 reports on the existence of a leeside centerline wake that is formed as a result of flow separation on the blunt nose of a body at moderate angles of attack (fig. 16(a)). The effect of nose shape is clearly seen by comparing the leeside vapor screens for a blunt-nose and a sharp-nose design of a monoplanar missile configuration having an elliptic body cross section. (See figs. 16(a) and 16(b), respectively.) Schlieren and vapor-screen photographs complement one another and are often used together in the flow analysis. Schlieren photographs, therefore, are also shown in figure 16 to aid in understanding the flow. A further investigation into the behavior of this centerline wake was initiated by using vapor-screen photographs for the basis of the study. The unusual behavior of this wake at model angle of attack and roll position is shown in figure 17. The analysis presented in reference 13 indicates that this leeside wake follows the upper-surface streamlines and becomes attached to the body vortex feed sheet. No known analytical methods are currently available for treatment of such complex flows; nor do any experimental methods exist for accurately measuring the properties of this complex flow. However, as a first step toward measurement and analysis, vapor-screen photographs, such as those in figure 17, can be used to understand the character of the flow.

Vapor-screen photographs have also been used in conjunction with surface pressures, oil flow, and tufts to classify separated-flow conditions on the upper surface of wings, as illustrated in figure 18. Both tuft and oil-flow photographs were used to determine surface flow direction. The tufts tend to reflect the velocity direction at the edge of the boundary layer, and oil streaks show the direction of flow on the surface. Only the vapor-screen flow-visualization technique provides flow-field information on the size, shape, and location of the vortex.

Vapor-screen results provided the basic information required to divide the flow on the upper surface of flat delta wings clearly into seven distinct flow classifications (ref. 14). Previously, only three flow classifications had been identified. Typical vapor-screen photographs of each of the seven conditions are shown in figure 19. The seven flow classifications have been identified as follows: (1) classical vortex, (2) vortex with shock, (3) separation bubble with no shock, (4) separation bubble with shock, (5) no shock/no separation, (6) shock with no separation, and (7) shock-induced separation. The analysis of reference 14 (made possible by high-quality vapor-screen photographs) provides guidance for the development of advanced theoretical methods as well as a means of explanation for wing behavior under separated-flow conditions.

Vapor-screen results can be greatly enhanced with the use of interactive graphics. An example of a computer-generated drawing of vortices produced by an elliptical body is illustrated in figure 20. To produce this illustration, the camera mounted inside the test section is used to provide several vapor-screen photographs at various body stations. The vortices at these body stations are then digitized and put into an interactive color-graphics display system that produces a very realistic three-dimensional vortex model using several colors to emphasize detail. This method allows the model with vortices to be viewed from any angle, thus providing pictorial illustrations for qualitative analysis.

CONCLUDING REMARKS

The vapor-screen technique for flow visualization in the Langley Unitary Plan Wind Tunnel (UPWT) has been presented with a description of the light sources and photographic equipment used. The tests have been conducted over the nominal operating speed range of the facility with a variation in light intensity, camera setting, and tunnel fog densities to determine the conditions required to obtain the optimum vapor-screen photographs.

The results show that the light intensity and camera setting, variation in tunnel dew point, Reynolds number, and tunnel stagnation temperature all have a significant effect on the quality of vapor-screen photographs.

A number of typical vapor-screen photographs of various flow patterns have been presented to illustrate both the quality of the photographs and how they are used in flow analysis.

The use of the vapor-screen technique in the UPWT, which complements the development of theoretical codes, has proven to be a valuable tool for interpreting complex three-dimensional flow fields.

NASA Langley Research Center
Hampton, VA 23665
April 30, 1985

REFERENCES

1. Spahr, J. Richard; and Dickey, Robert R.: Wind-Tunnel Investigation of the Vortex Wake and Downwash Field Behind Triangular Wings and Wing-Body Combinations at Supersonic Speeds. NACA RM A53D10, 1953.

2. [illegible]cynski, John P.: An Experimental Investigation of the Flow Phenomena Over [illegible]dies at High Angles of Attack at a Mach Number of 2.01. NACA RM L55 H29, 1[illegible]5.

3. Nietubicz, Charles J.: Vapor Screen Technique Development at the Ballistic Research Laboratories. BRL Memo. Rep. No. 2387, U.S. Army, June 1974. (Available from DTIC as AD 784 077.)

4. Monta, William J.: Supersonic Aerodynamic Characteristics of a Sparrow III Type Missile Model With Wing Controls and Comparison With Existing Tail-Control Results. NASA TP-1078, 1977.

5. Graves, Ernald B.: Aerodynamic Characteristics of a Monoplanar Missile Concept With Bodies of Circular and Elliptical Cross Sections. NASA TM-74079, 1977.

6. Landrum, Emma Jean; and Babb, C. Donald: Wind-Tunnel Force and Flow-Visualization Data at Mach Numbers From 1.6 to 4.63 for a Series of Bodies of Revolution at Angles of Attack From -4° to 60°. NASA TM-78813, 1979.

7. Robins, A. Warner; Lamb, Milton; and Miller, David S.: Aerodynamic Characteristics at Mach Numbers of 1.5, 1.8, and 2.0 of a Blended Wing-Body Configuration With and Without Integral Canards. NASA TP-1427, 1979.

8. Stallings, Robert L., Jr.; Lamb, Milton; and Watson, Carolyn B.: Effect of Reynolds Number on Stability Characteristics of a Cruciform Wing-Body at Supersonic Speeds. NASA TP-1683, 1980.

9. Jackson, Charlie M., Jr.; Corlett, William A.; and Monta, William J.: Description and Calibration of the Langley Unitary Plan Wind Tunnel. NASA TP-1905, 1981.

10. Hill, J. A. F.; Baron, J. R.; Schindel, L. H.; and Markham, J. R.: Mach Number Measurements in High-Speed Wind Tunnels. AGARDograph 22, Oct. 1956.

11. Allen, Jerry M.; and Dillenius, Marnix F. E.: Vortex Development on Slender Missiles at Supersonic Speeds. J. Spacecr. & Rockets, vol. 17, no. 4, July-Aug. 1980, pp. 377-381.

12. Graves, Ernald B.; and Robins, A. Warner: Supersonic Aerodynamic Trade Data for a Low-Profile Monoplanar Missile Concept. AIAA Paper 79-0222, Jan. 1979.

13. Allen, Jerry M.; and Pittman, Jimmy L.: Analysis of Surface Pressure Distributions on Two Elliptic Missile Configurations. AIAA-83-1841, July 1983.

14. Miller, David S.; and Wood, Richard M.: An Investigation of Wing Leading-Edge Vortices at Supersonic Speeds. AIAA-83-1816, July 1983.

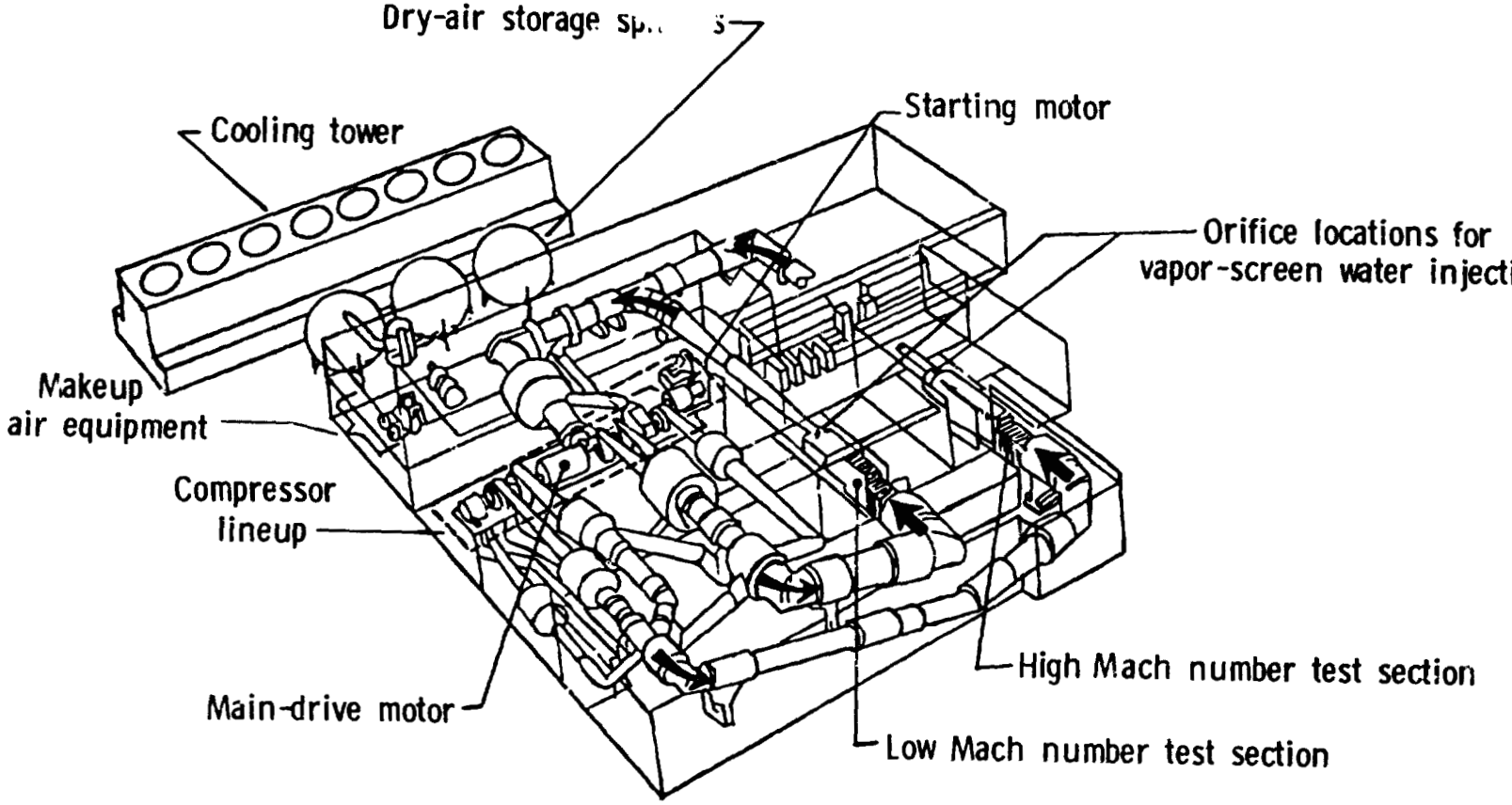

Figure 1.- Schematic drawing of the Langley Unitary Plan Wind Tunnel (UPWT). Orifice locations for vapor-screen water injection are indicated.

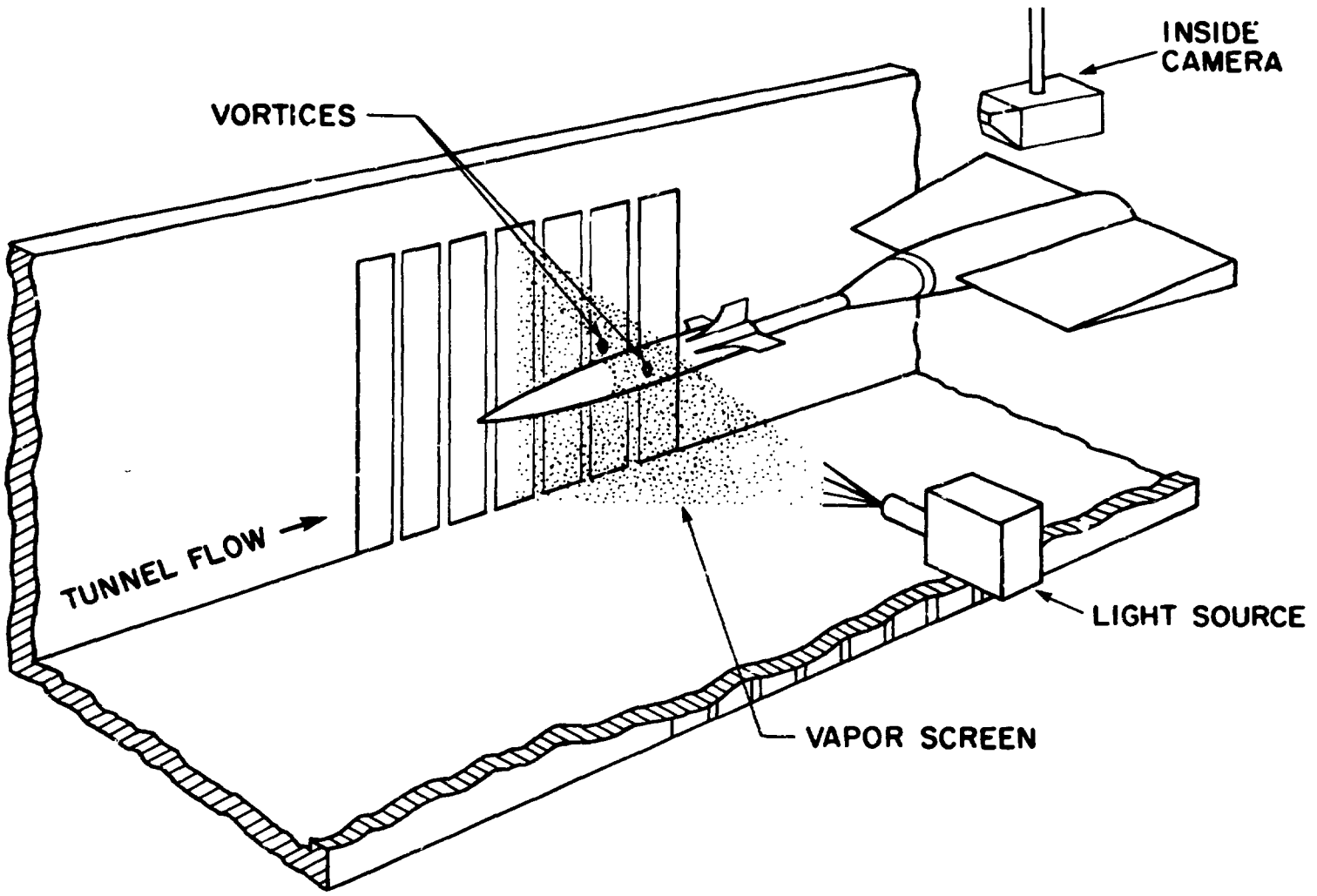

(a) Vapor-screen technique.

Figure 2.- Sketch of vapor-screen apparatus.

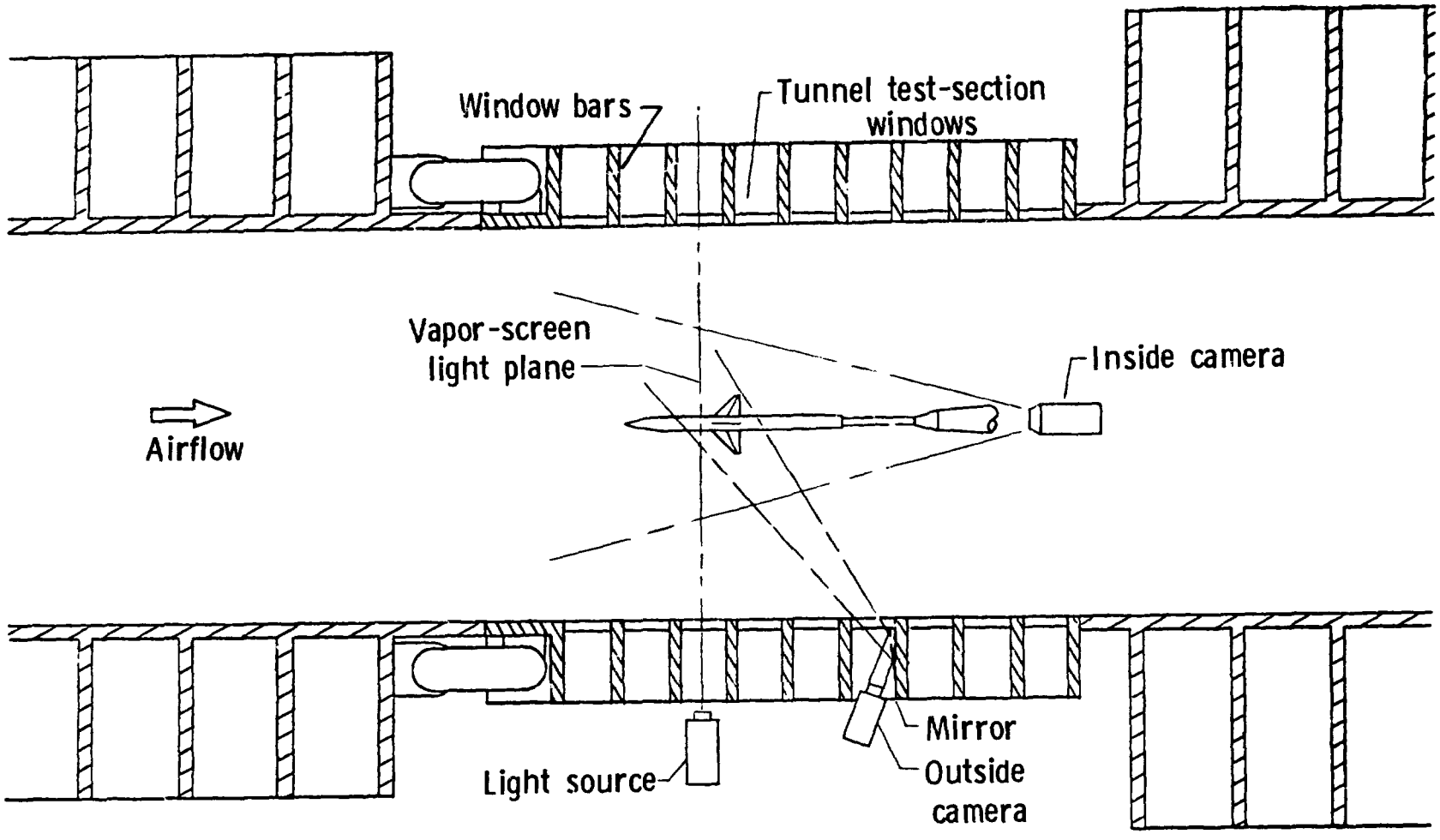

(b) Vapor-screen equipment in the UPWT.

Figure 2.- Continued.

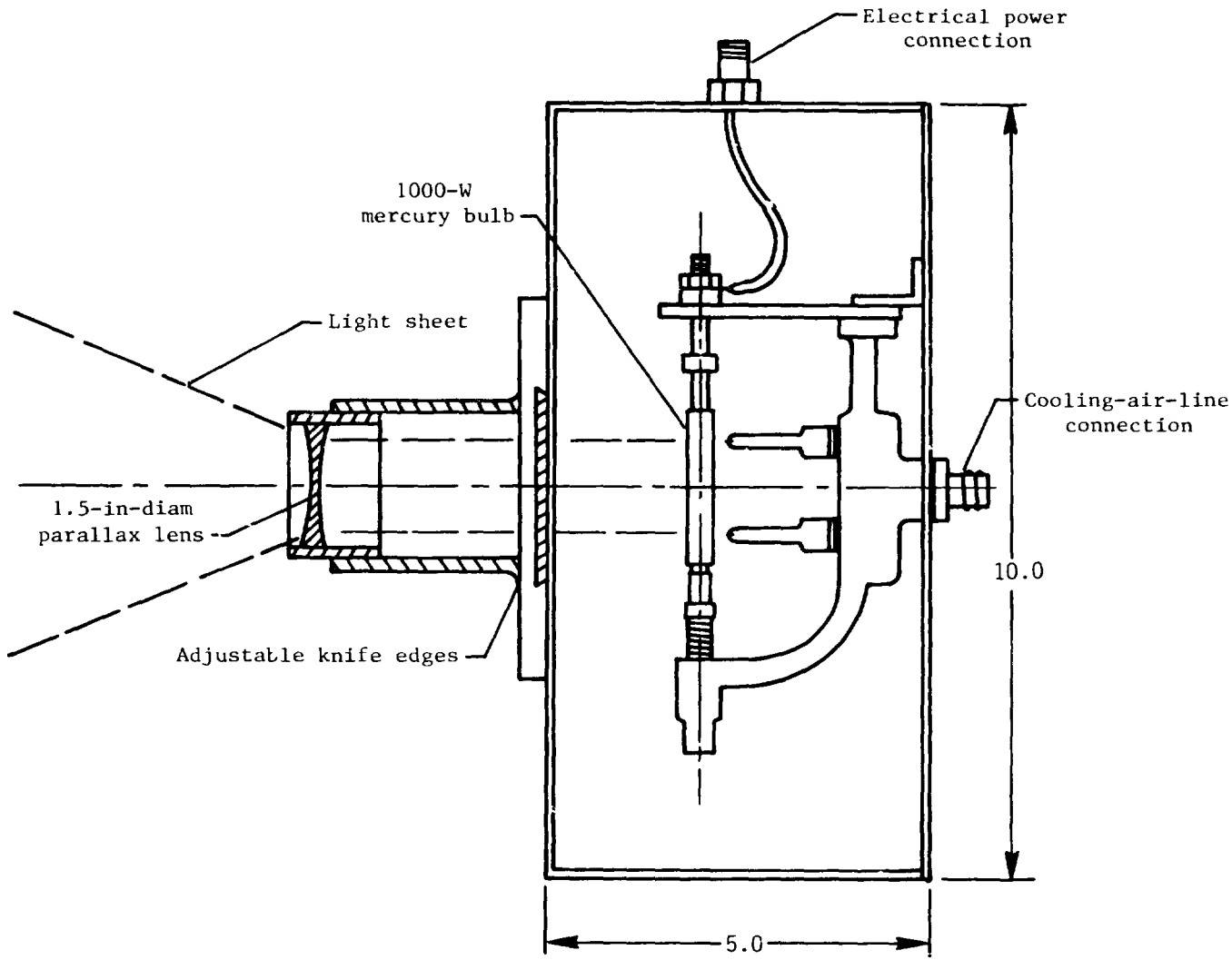

(c) Details of 1000-W mercury-vapor lamp. All dimensions are given in inches unless otherwise specified.

Figure 2.- Concluded.

L-77-6067

(a) Test section 1.

Figure 3.- Photograph of model and inside camera mounted in the UPWT.

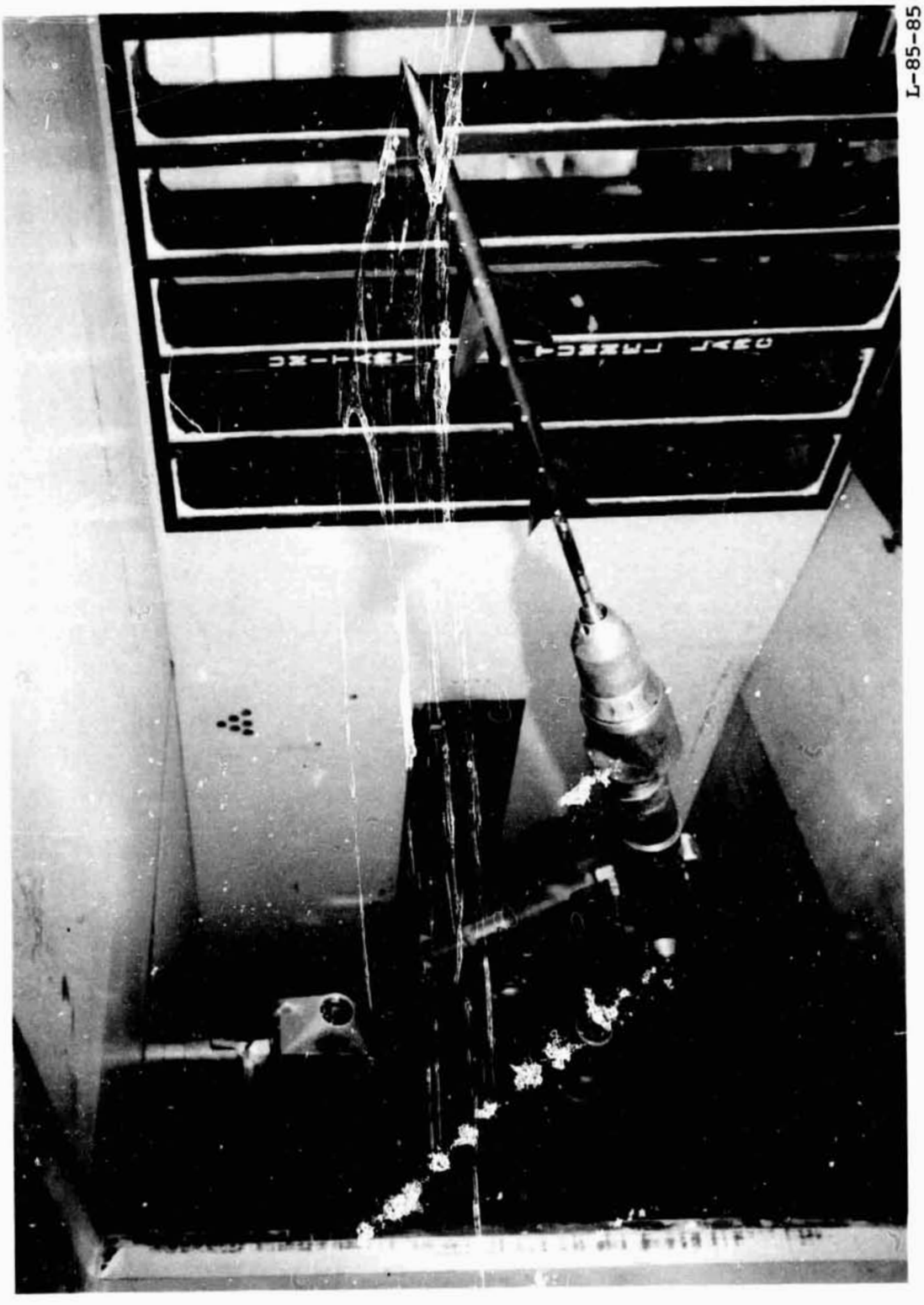

L-85-85

(b) Test section 2.

Figure 3.- Concluded.

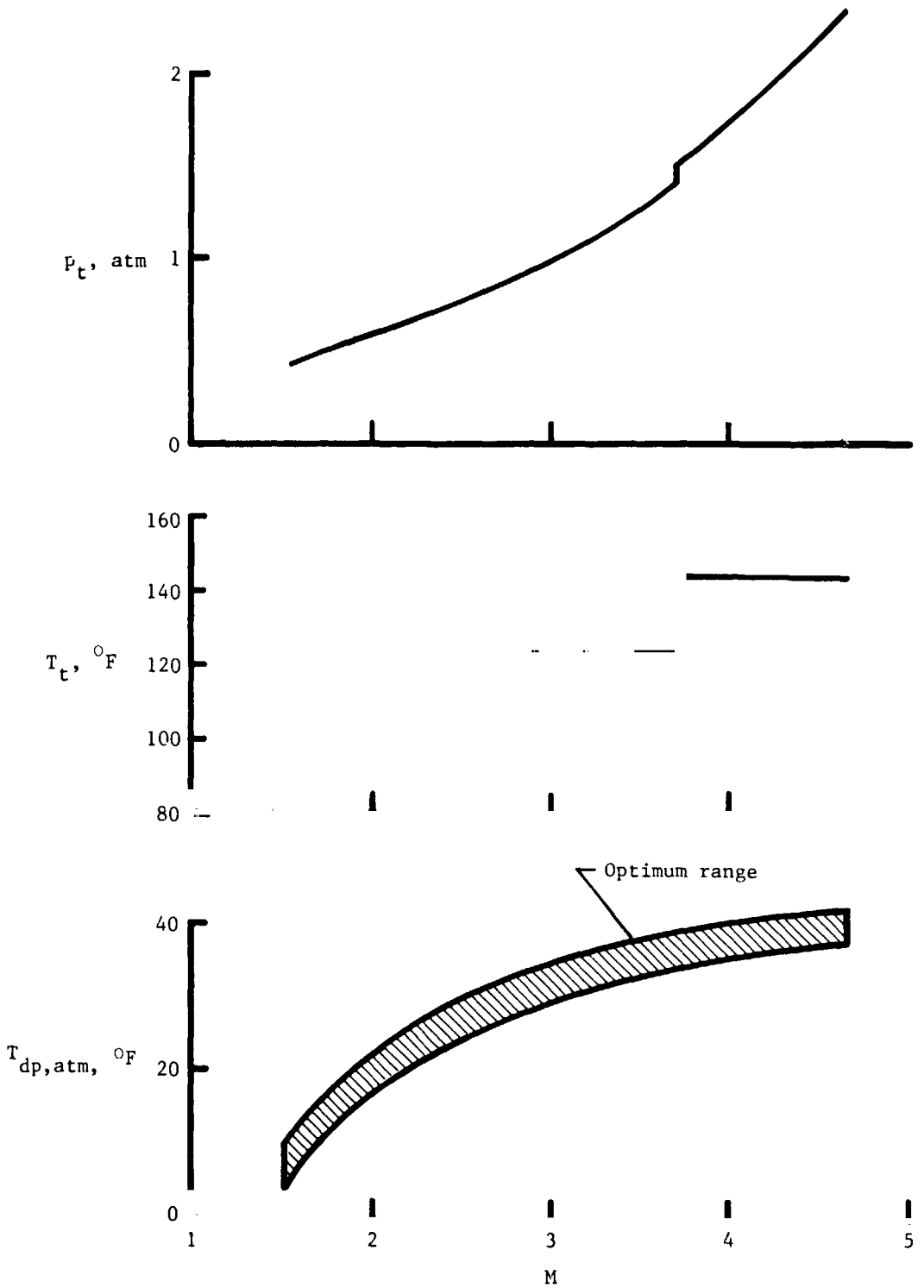

Figure 4.- Tunnel operating conditions for optimum vapor screen at nominal test unit Reynolds number of 2.0×10^6 per foot. Mach number range includes both test sections.

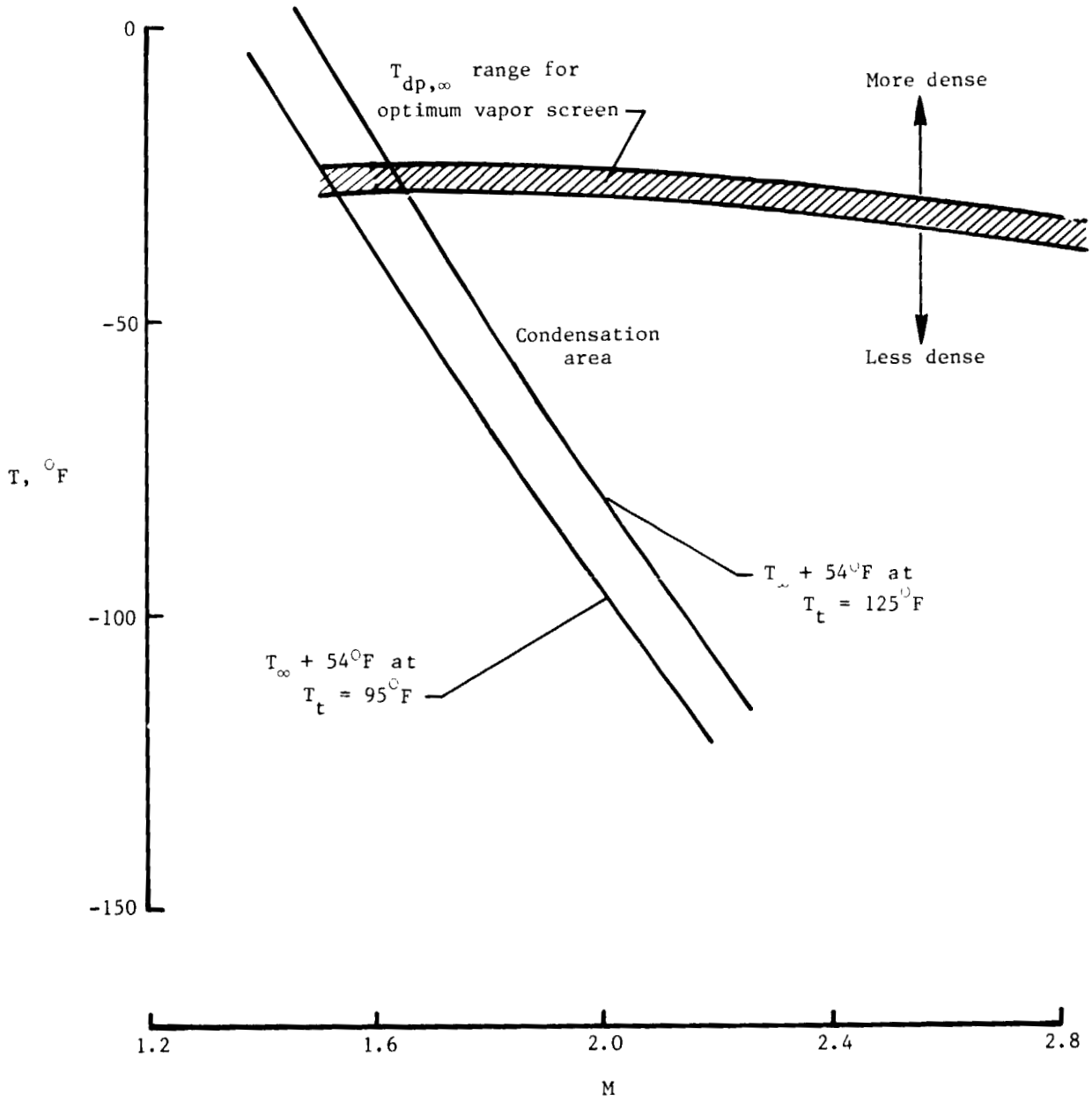

Figure 5.- Comparison of vapor-screen dew-point values with condensation boundaries (assuming a supercooling increment of 54°F). R = 2.0×10^6 per foot.

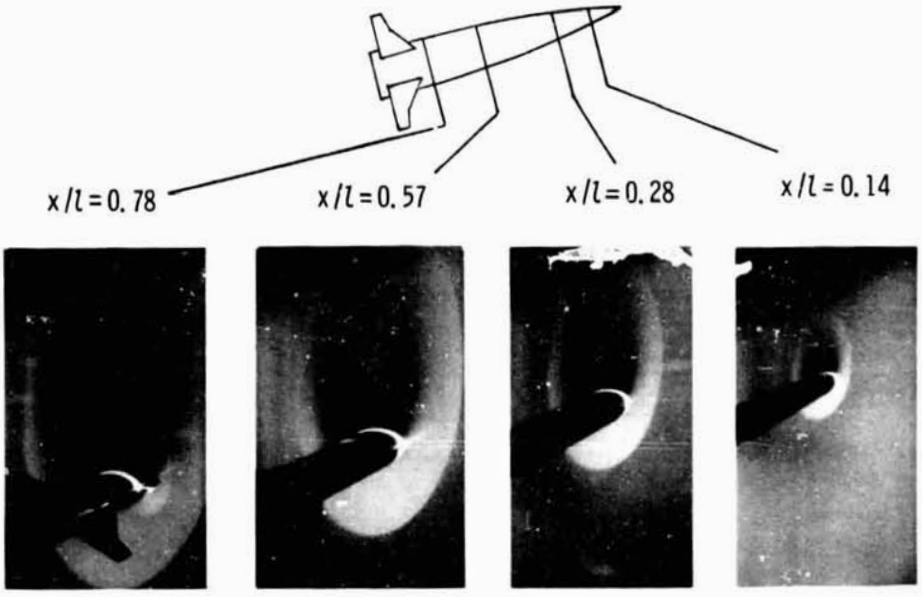

(a) Single light from right side.

(b) Single light from left side.

(c) Lights from both sides.

L-85-86

Figure 6.- Effect of light-source location on vapor-screen photographs (camera on right side). M = 2.96; α = 22°.

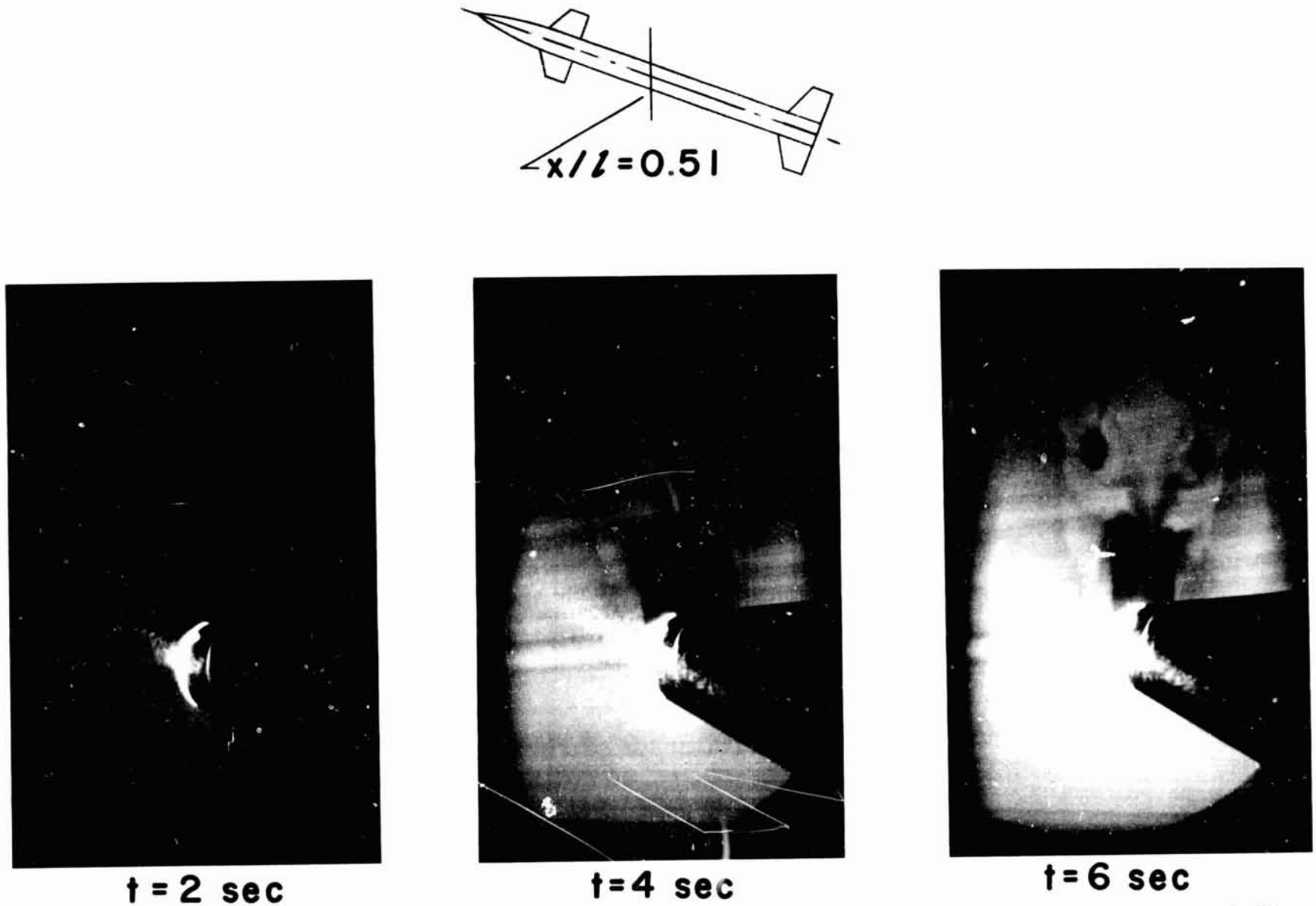

Figure 7.- Vapor-screen photographs using 15-mW laser light source.
M = 2.86; α = 20.2°.

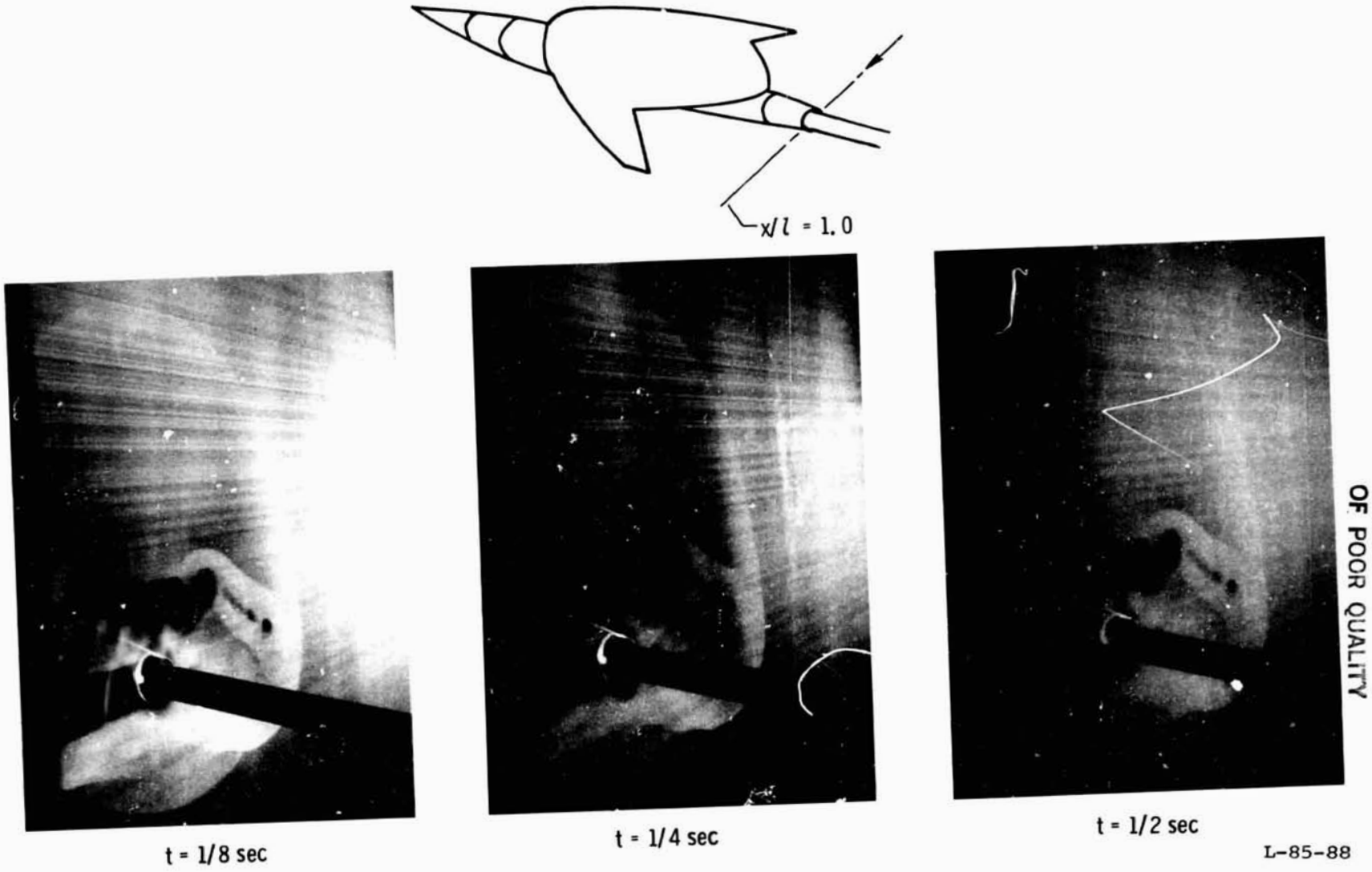

Figure 8.- Vapor-screen photographs of wing-body model using 4-W laser light source. $M = 4.5$; $\alpha = 12°$.

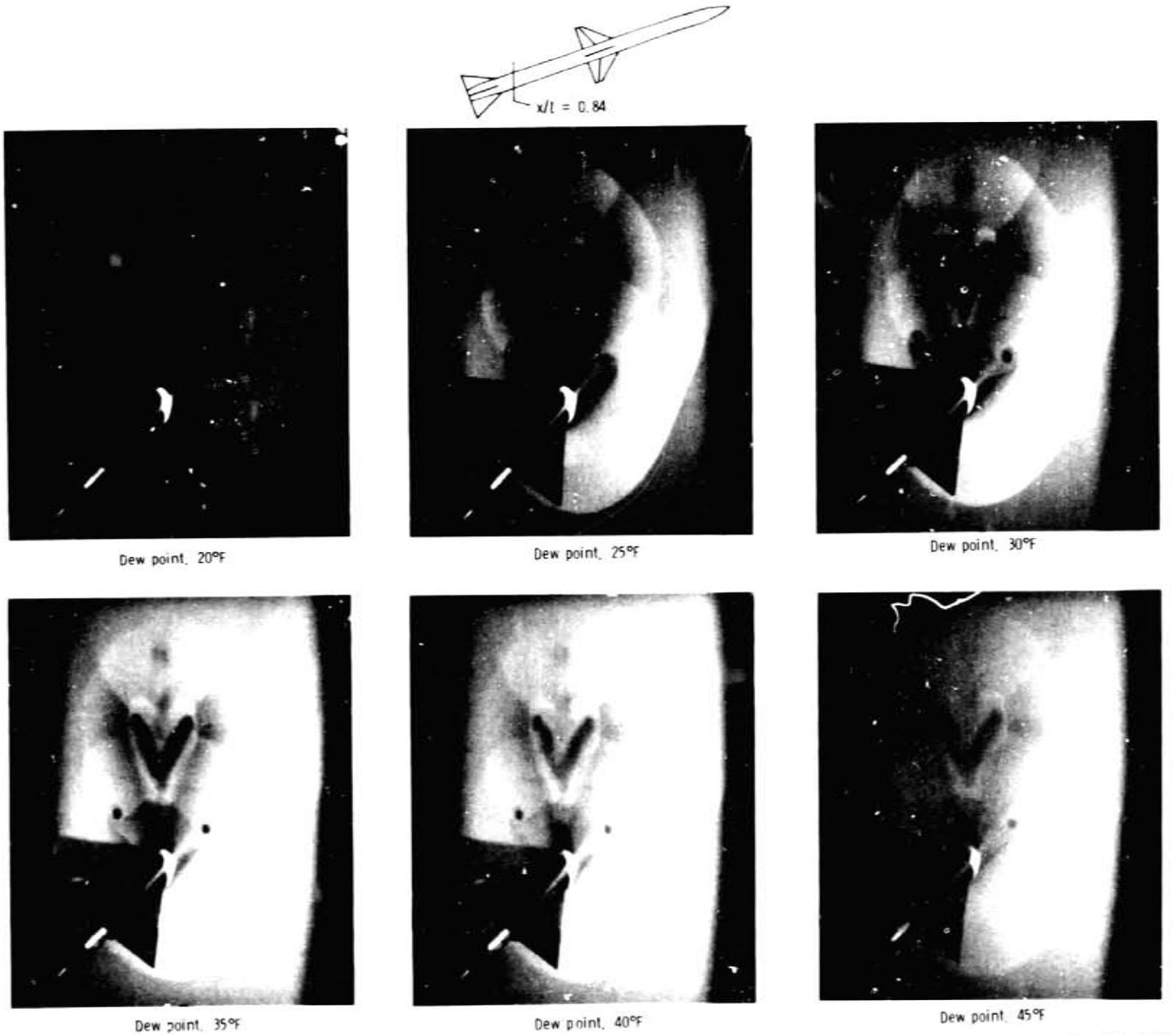

Figure 9.- Effect of dew point on vapor-screen photographs. M = 2.35; R = 2.0×10^6 per foot; T_t = 150°F; α = 35°; ϕ = 45°.

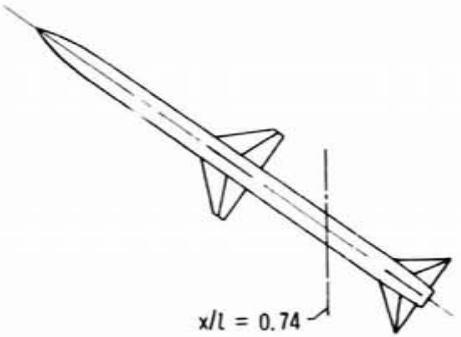

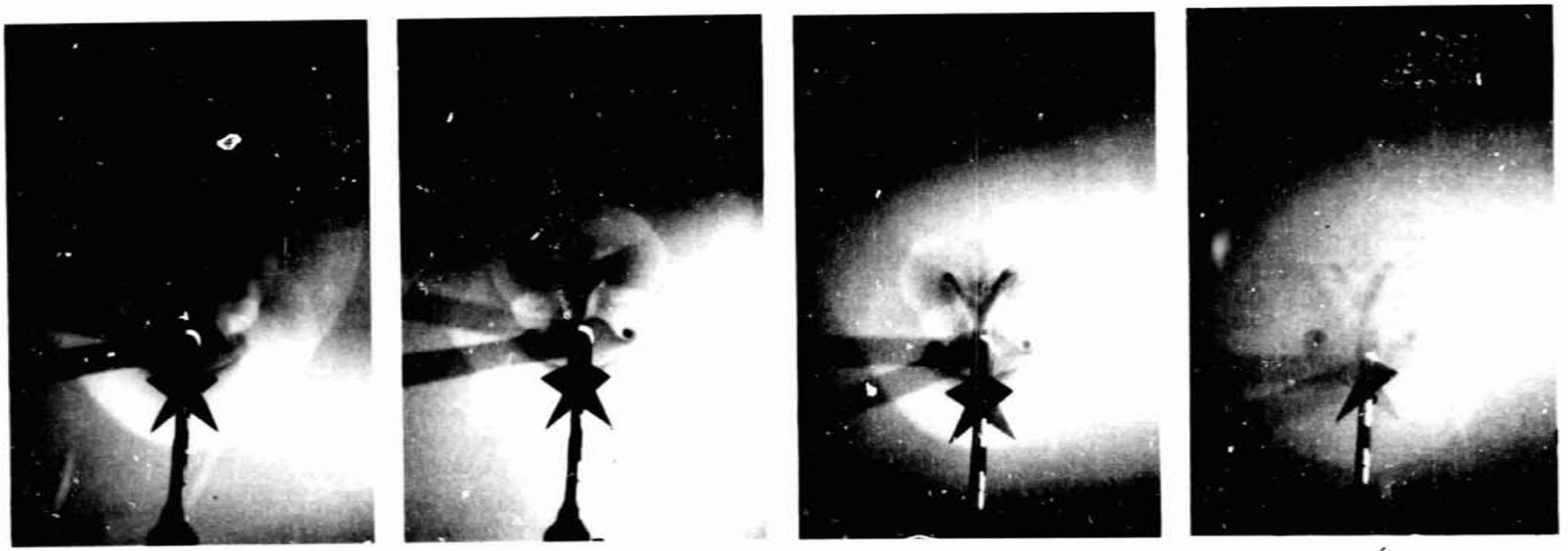

R = 1.0 × 10^6 per foot

R = 2.0 × 10^6 per foot

R = 3.0 × 10^6 per foot

R= 4.0 × 10^6 per foot

L-85-90

Figure 10.- Effect of Reynolds number on vapor-screen photographs. M = 2.35; dew point, 30°F; T_t = 150°F; α = 35°; ϕ = 45°.

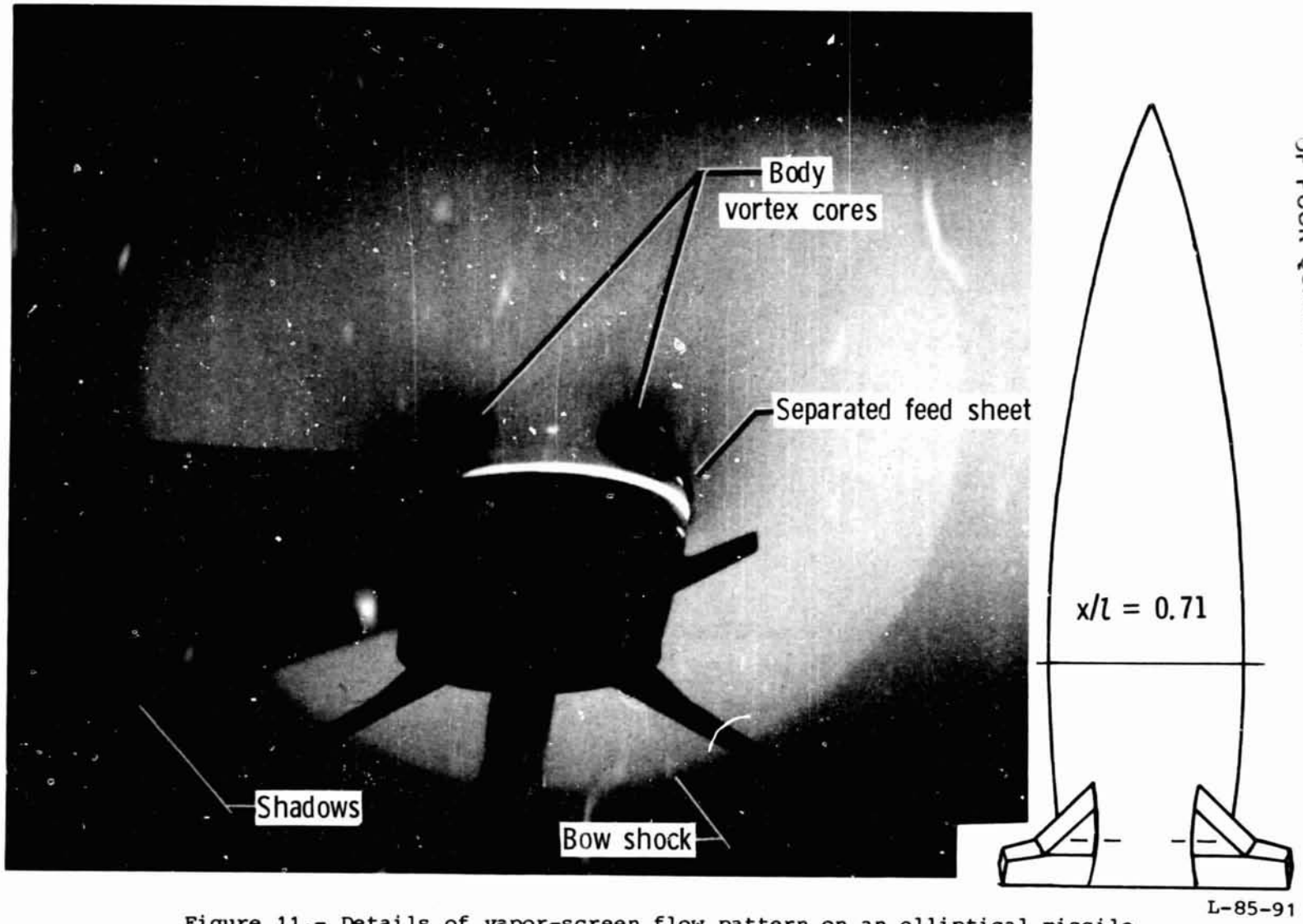

Figure 11.- Details of vapor-screen flow pattern on an elliptical missile model. $M = 2.6$; $\alpha = 26°$; $\phi = 0°$.

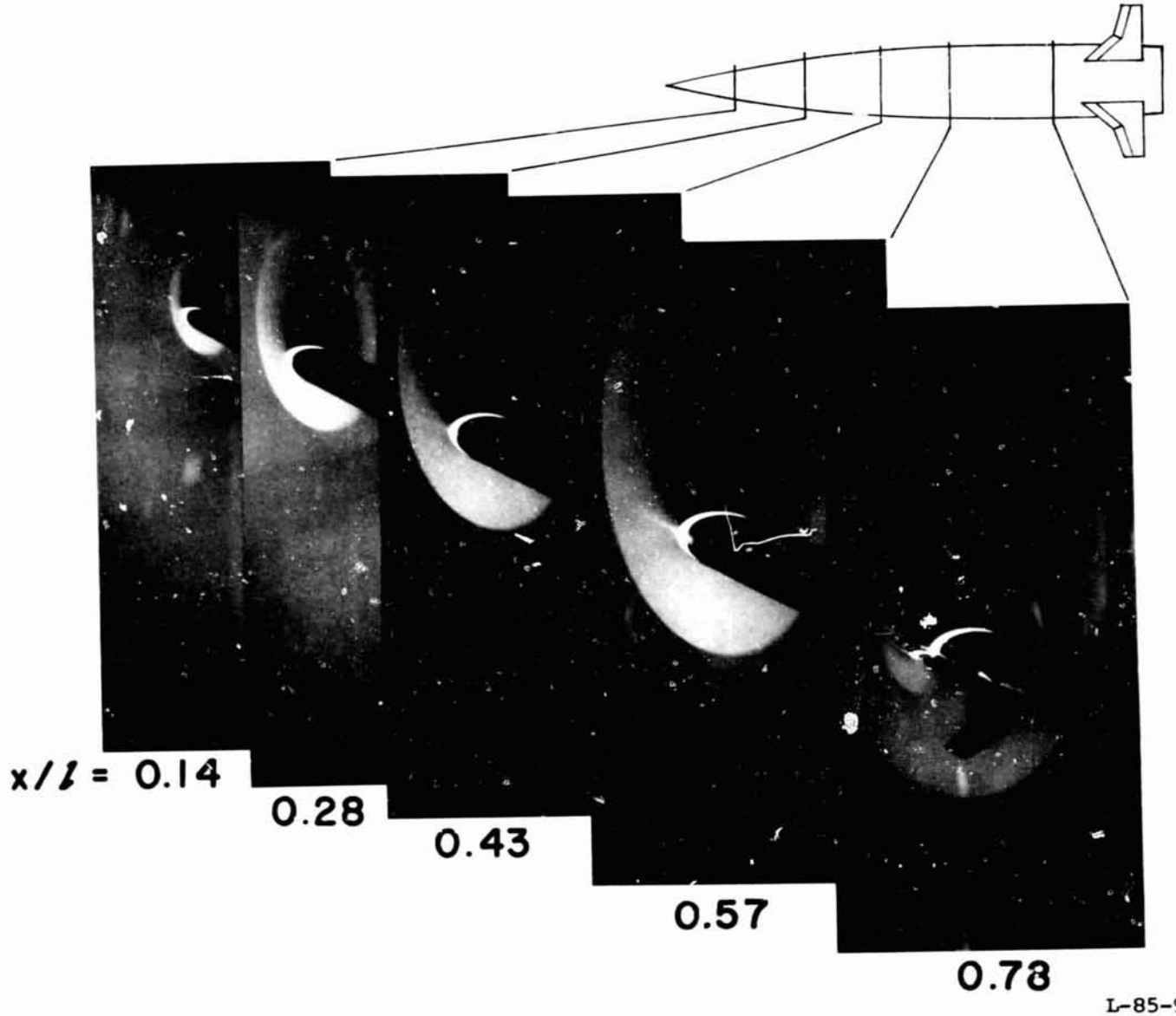

(a) Outside camera. M = 2.86; α = 22°; ϕ = 0°.

Figure 12.- Vapor-screen photographs comparing camera locations.

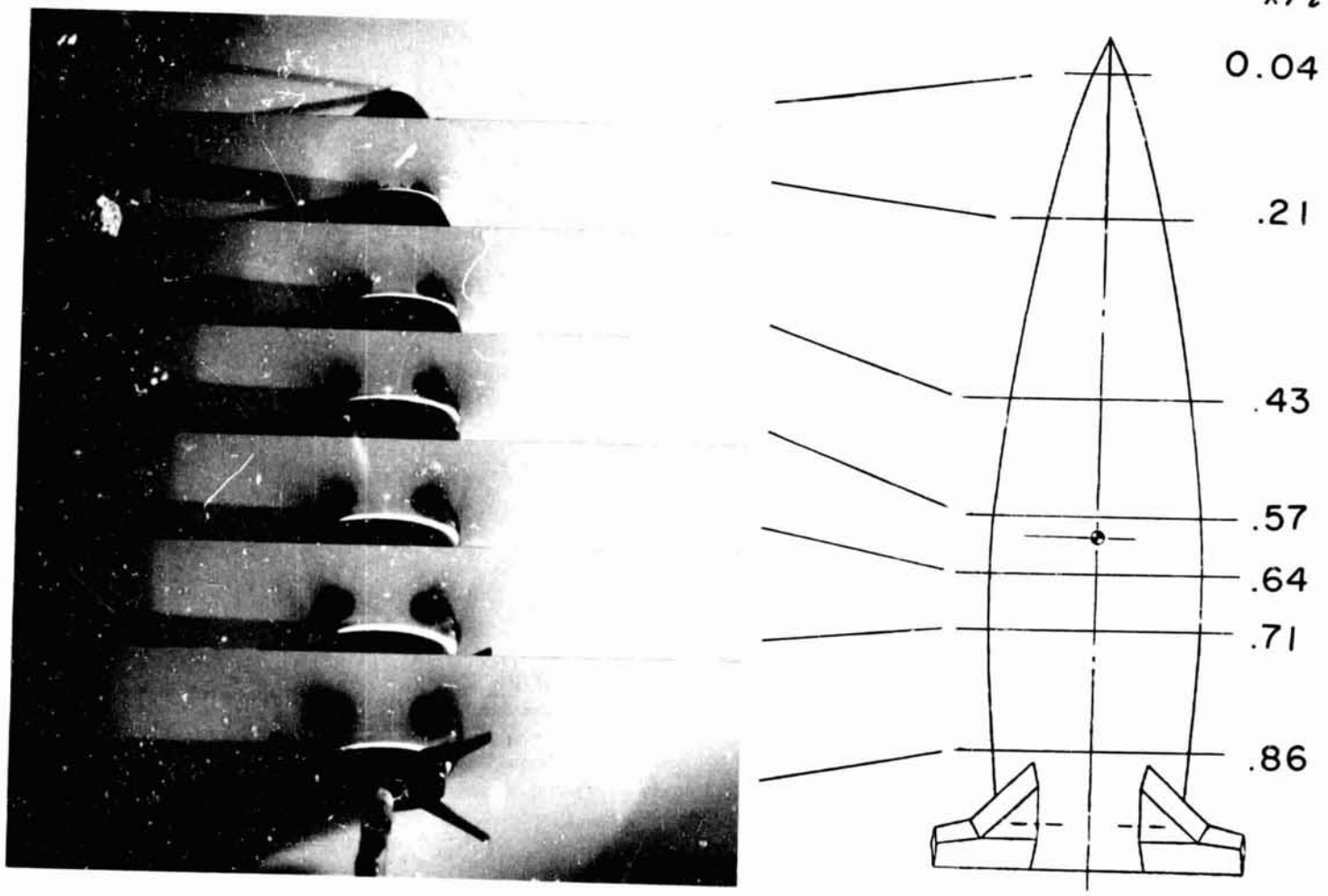

(b) Inside camera. M = 2.6; α = 26°; ϕ = 0°.

Figure 12.- Concluded.

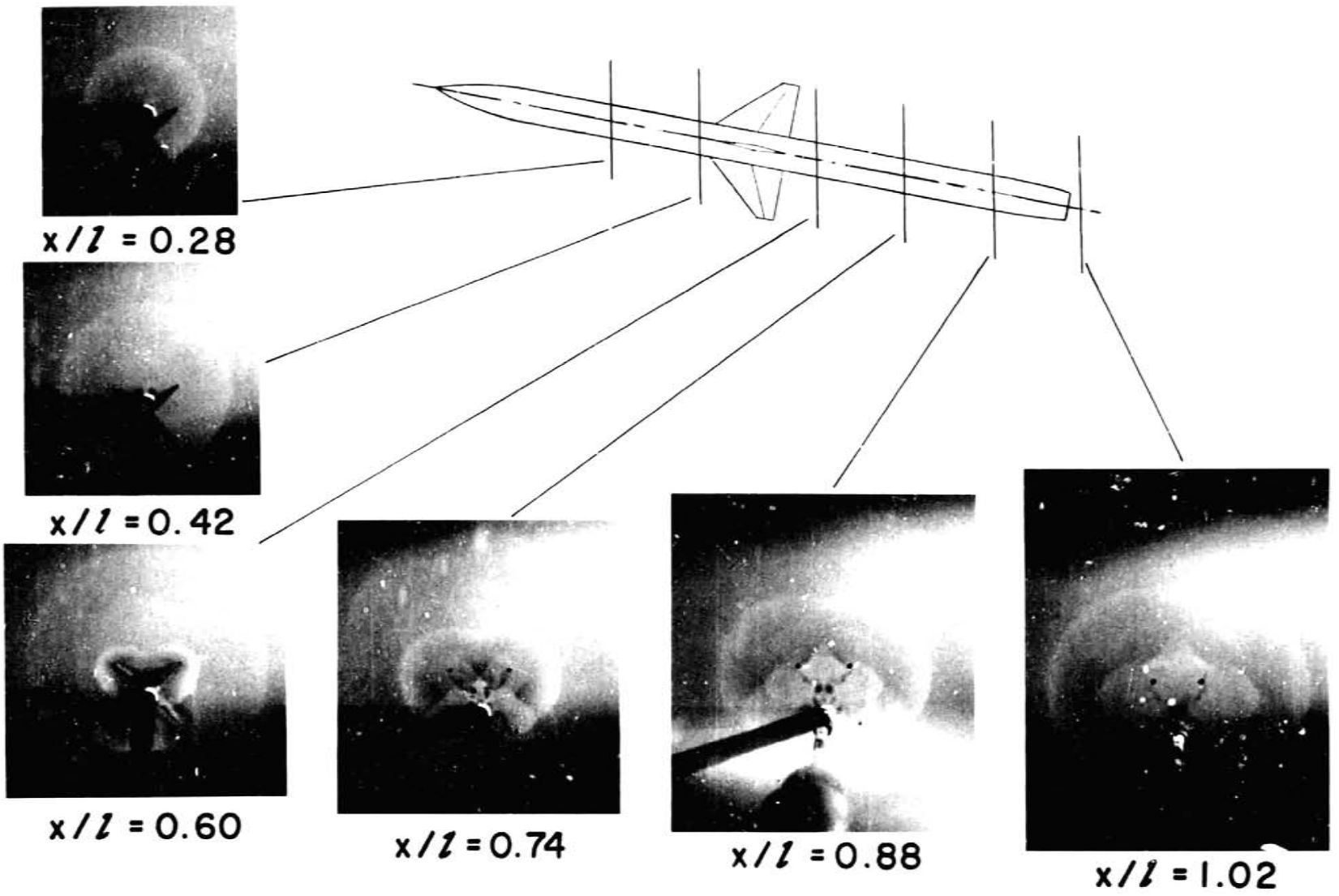

(a) $\alpha = 11.5°$.

Figure 13.- Vapor-screen photographs of flow patterns of cruciform missile model at several chordwise stations. M = 2.35; $\phi = 45°$.

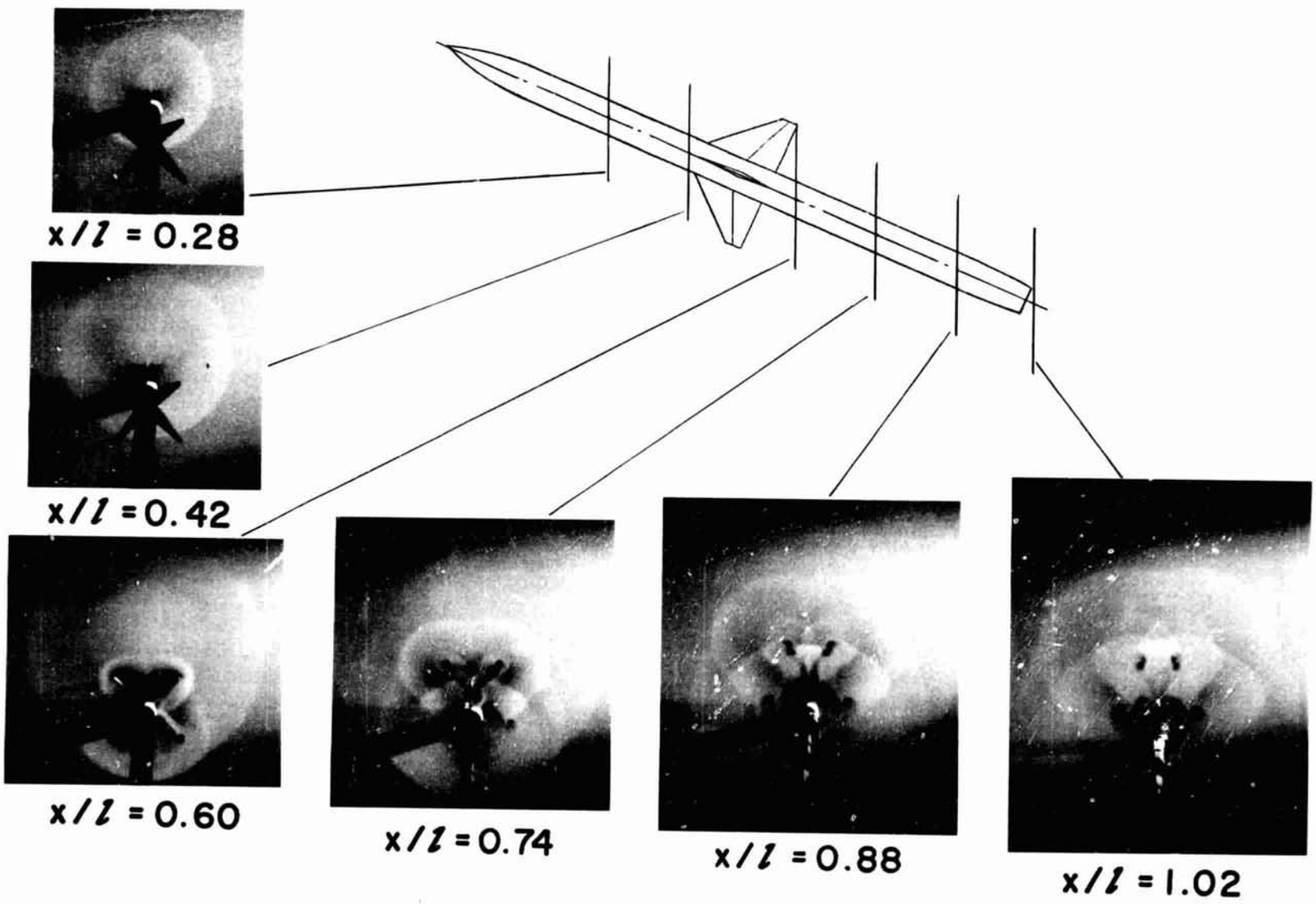

(b) $\alpha = 23.2°$.

Figure 13.- Continued.

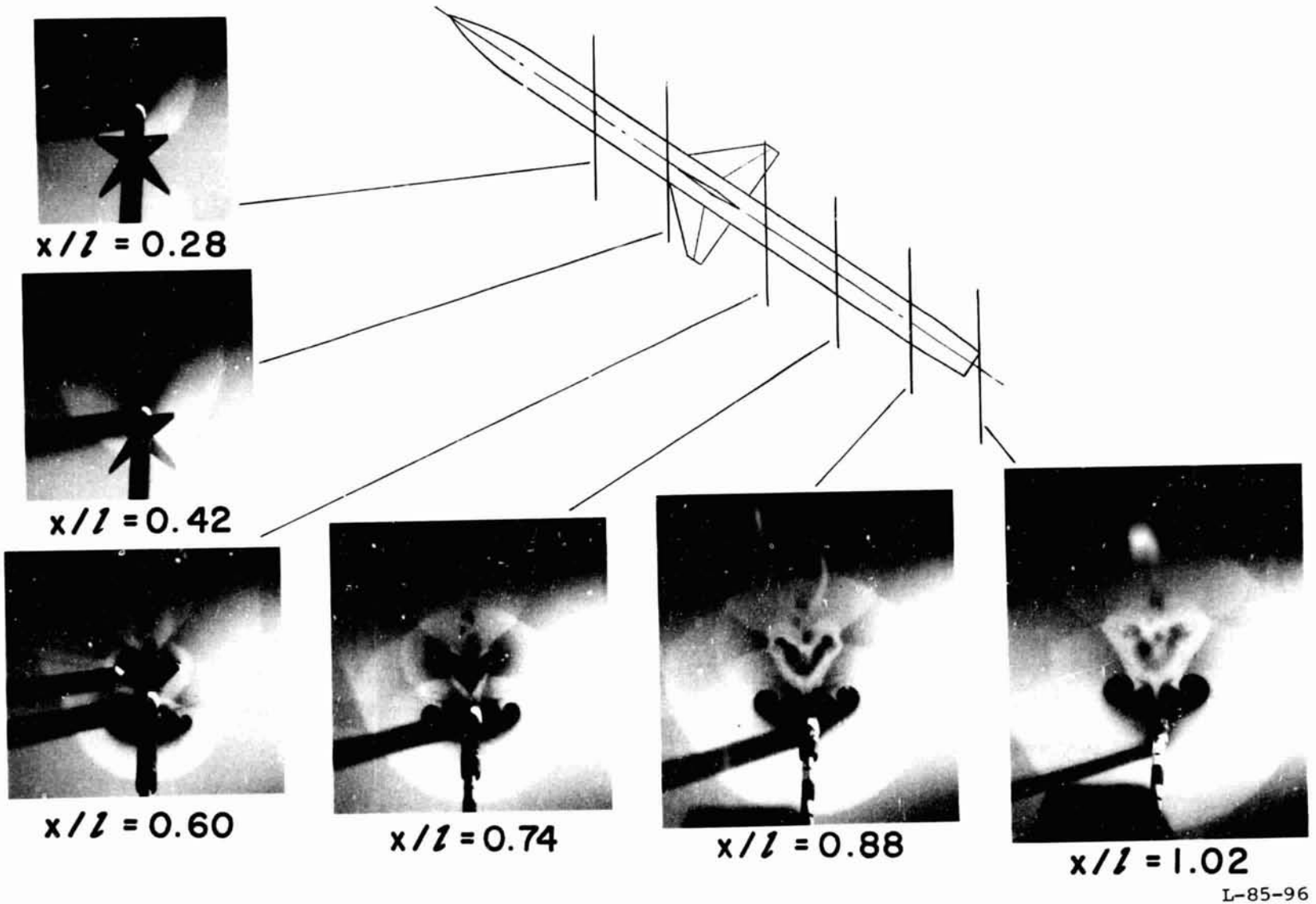

(c) $\alpha = 35.2°$.

Figure 13.- Concluded.

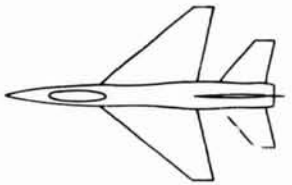

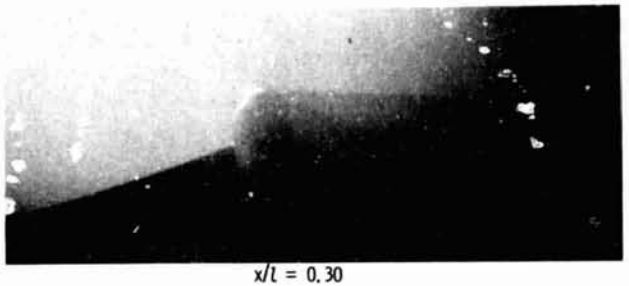

x/l = 0.30

x/l = 0.82

x/l = 0.45

x/l = 0.90

x/l = 0.60

x/l = 1.12

L-85-97

(a) $\alpha = 3°$.

Figure 14.- Vapor-screen photographs of flow patterns of fighter-type airplane configuration. M = 1.8.

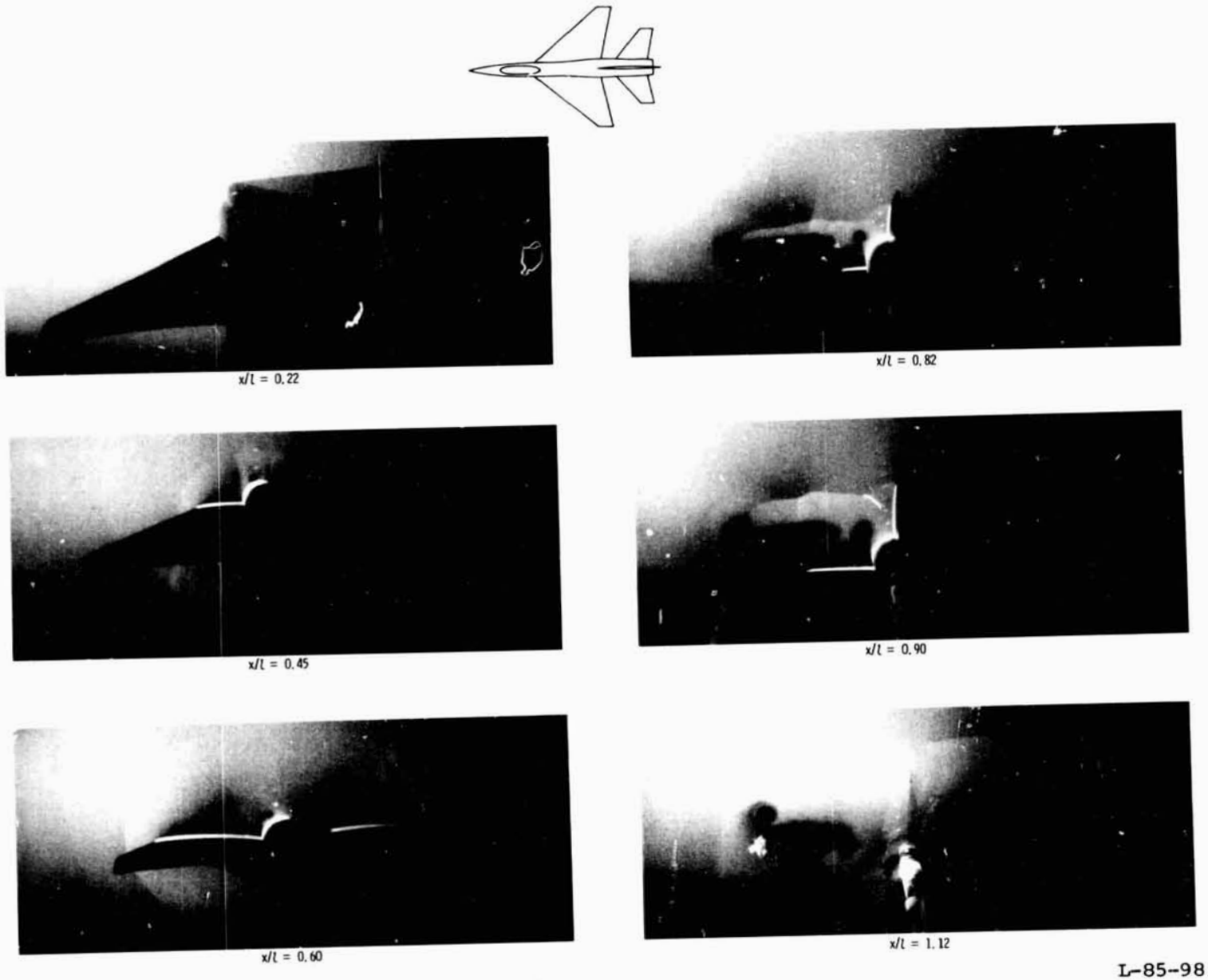

L-85-98

(b) $\alpha = 10°$.

Figure 14.- Concluded.

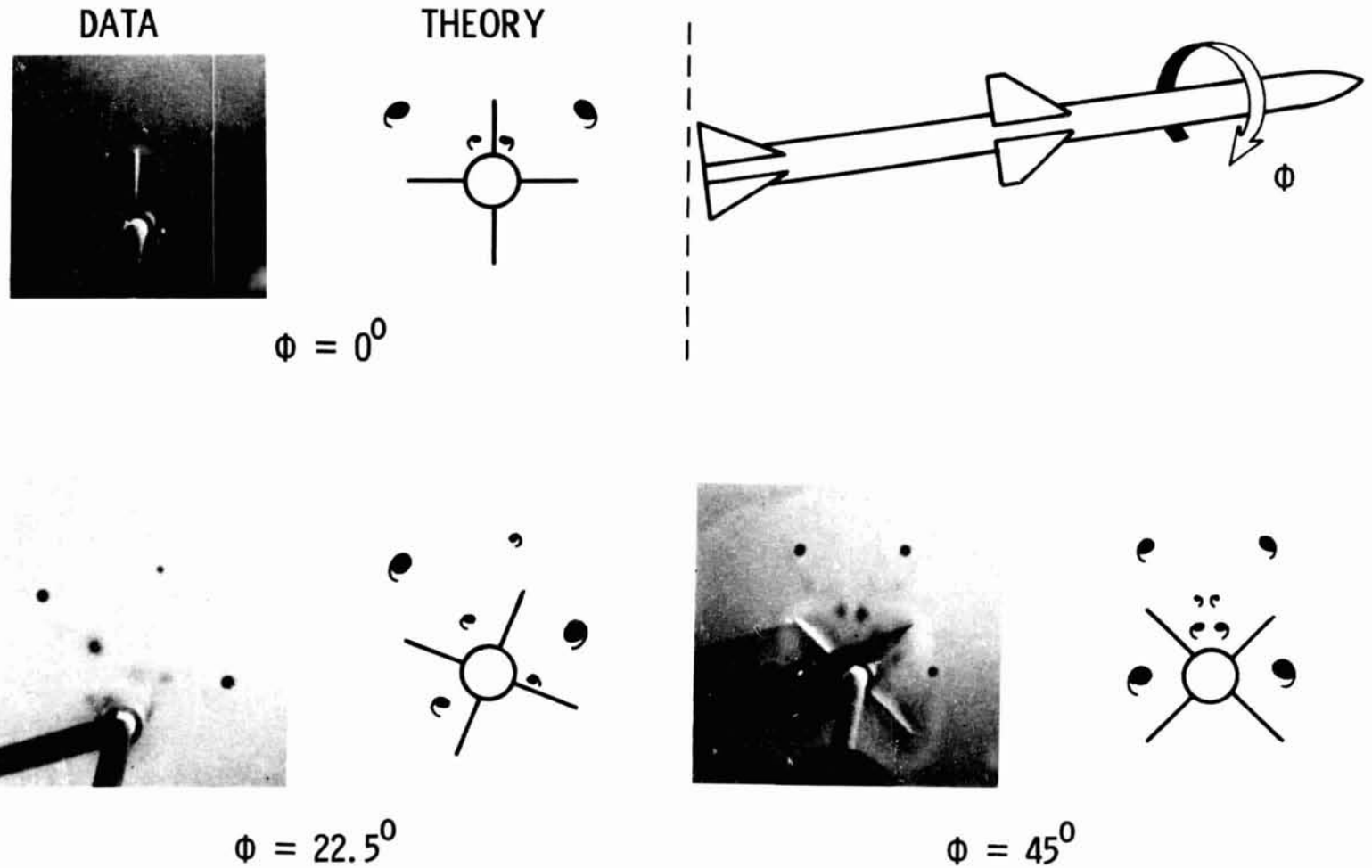

L-85-99

Figure 15.- Effect of roll angle on vortex patterns (from ref. 11).
$\alpha = 11.4°$; $x/l = 1.02$.

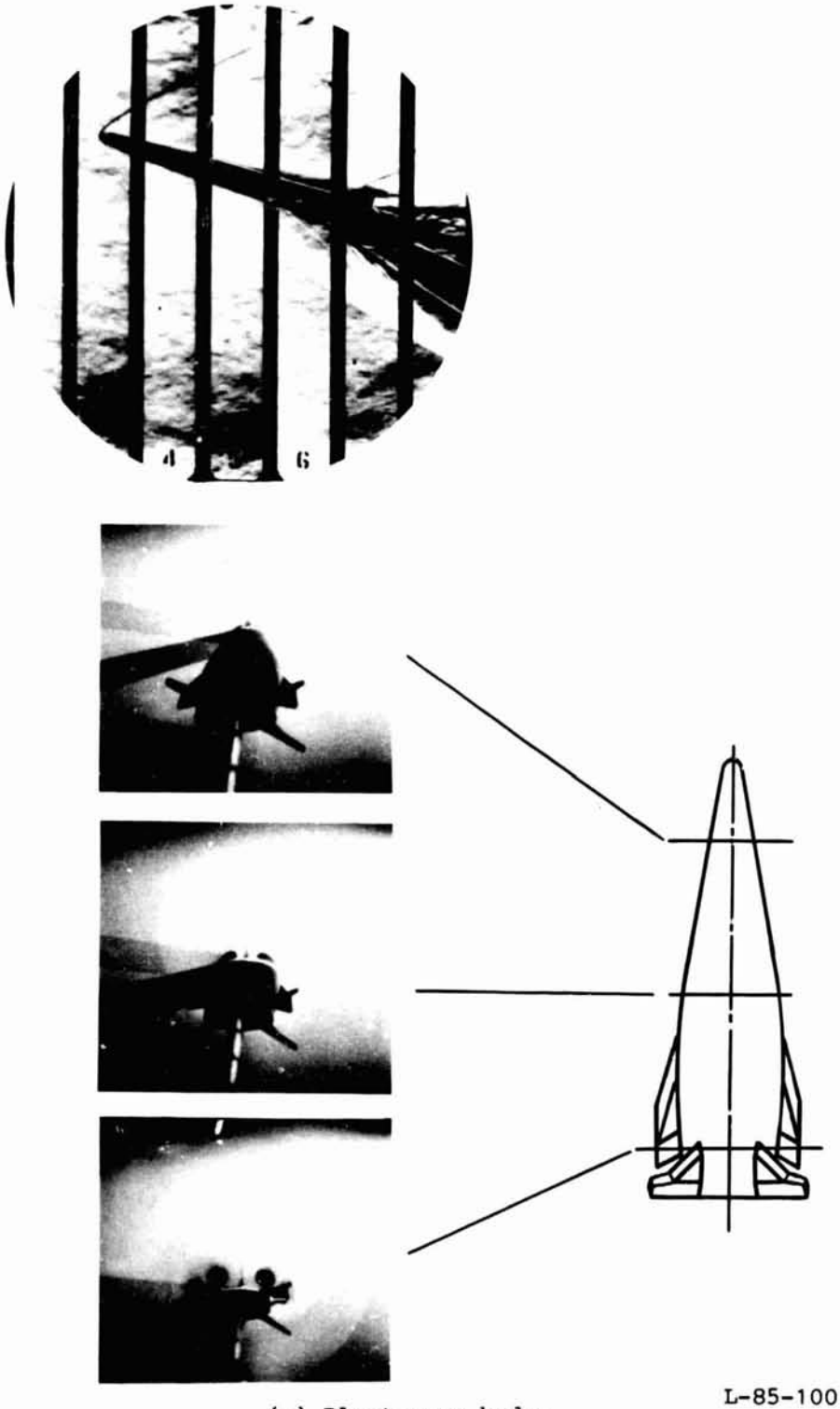

L-85-100

(a) Blunt-nose body.

Figure 16.- Vapor-screen photographs of elliptic monoplanar missile (from ref. 12). M = 2.5; α = 15°.

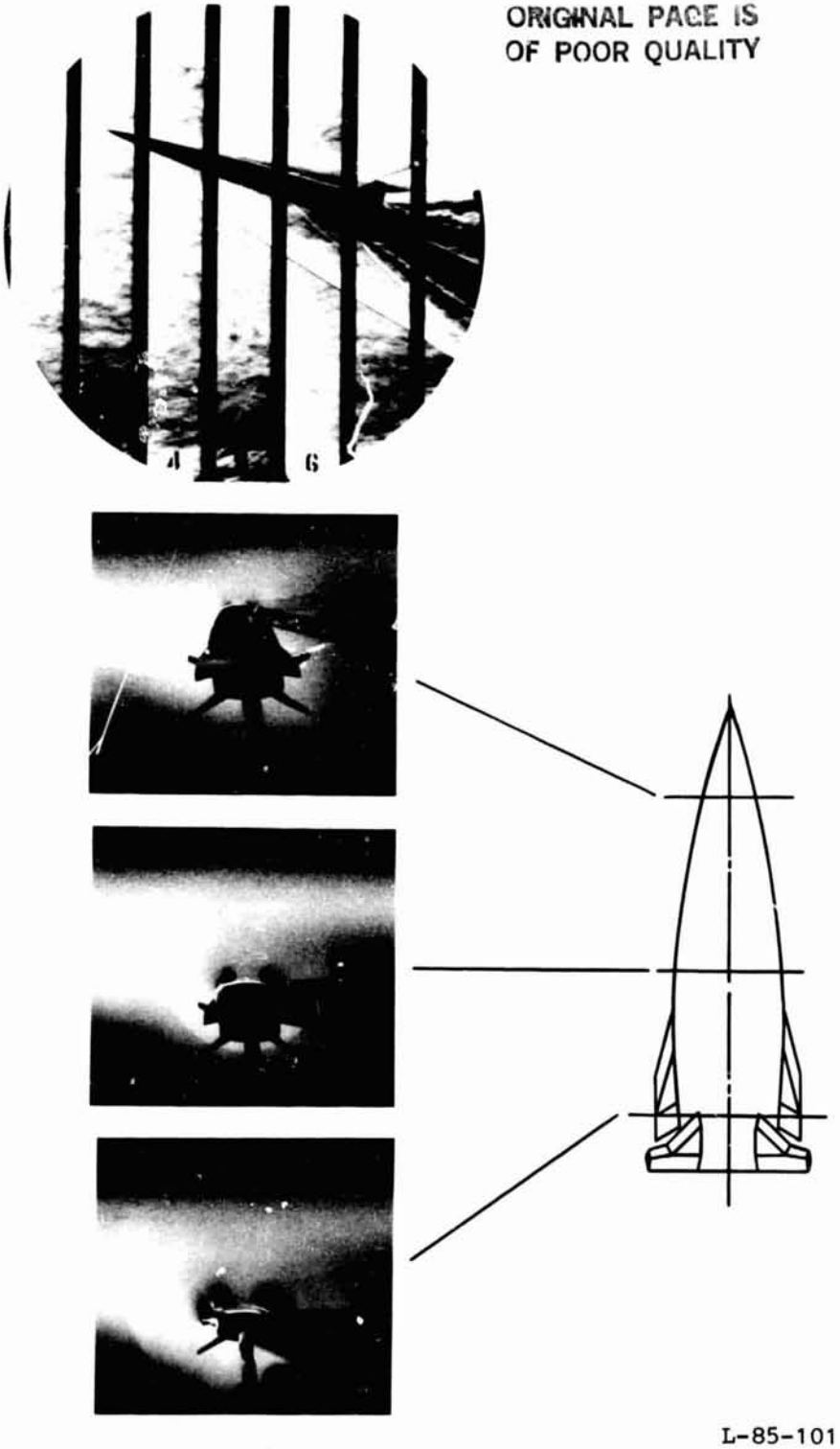

L-85-101

(b) Sharp-nose body.

Figure 16.- Concluded.

Vapor-screen photographs

Computer graphics

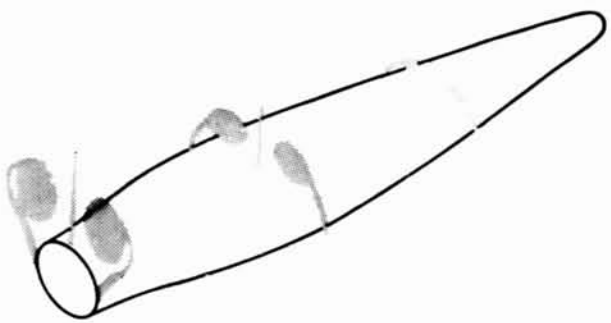

(a) $x/l = 0.32$; $\phi = 0°$.

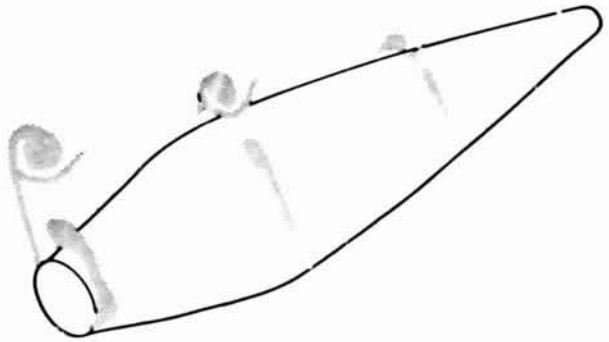

(b) $x/l = 1.0$; $\phi = 45°$.

L-82-10,774

Figure 17.- Vortex patterns on blunt-nose body (from ref. 13). $M = 2.5$; $\alpha = 20°$.

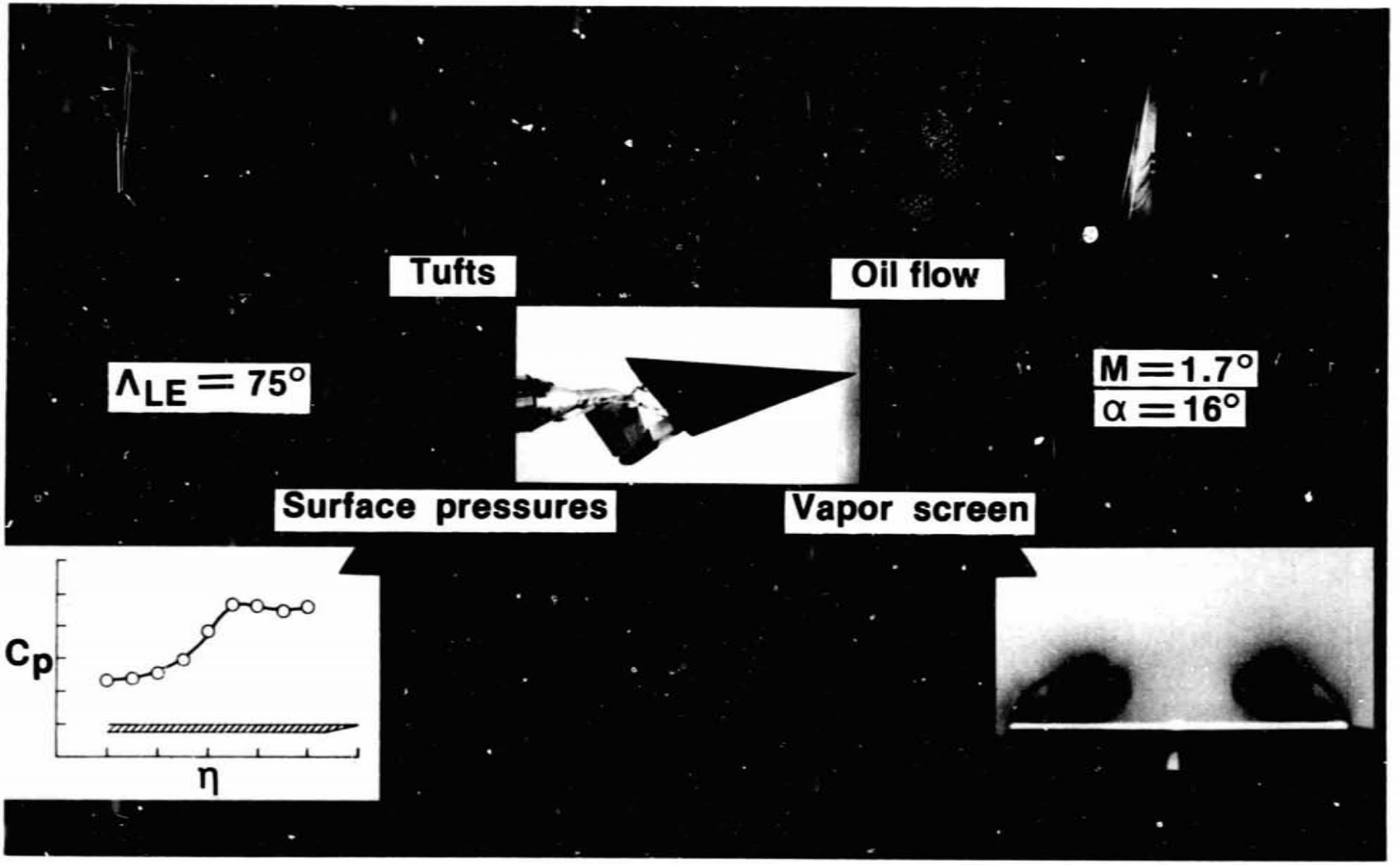

L-83-8123

Figure 18.- Experimental data used to evaluate flow on leeside of delta wing (from ref. 14).

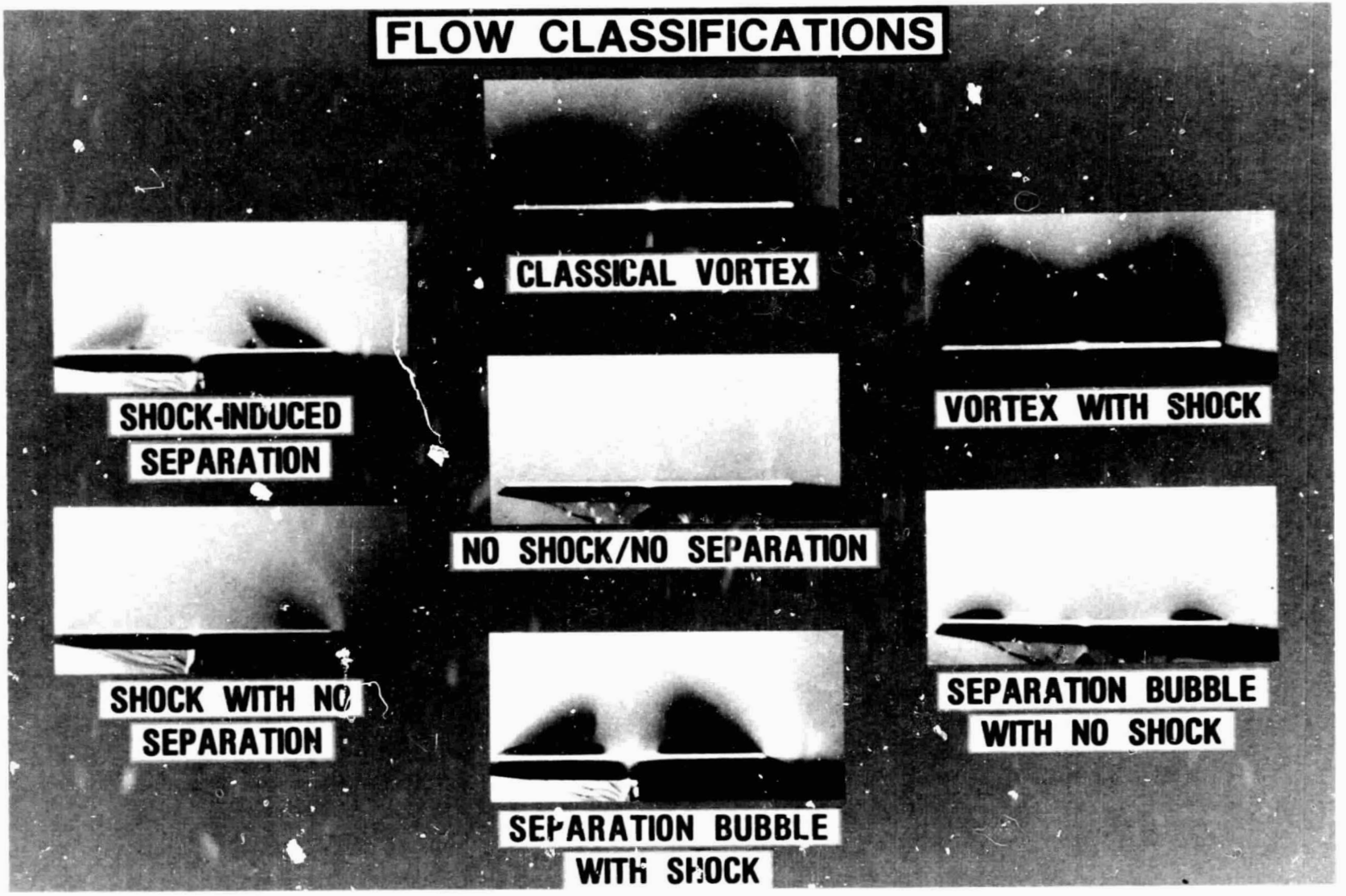

L-83-8124

Figure 19.- Flow classifications over delta wing using vapor screen (from ref. 14).

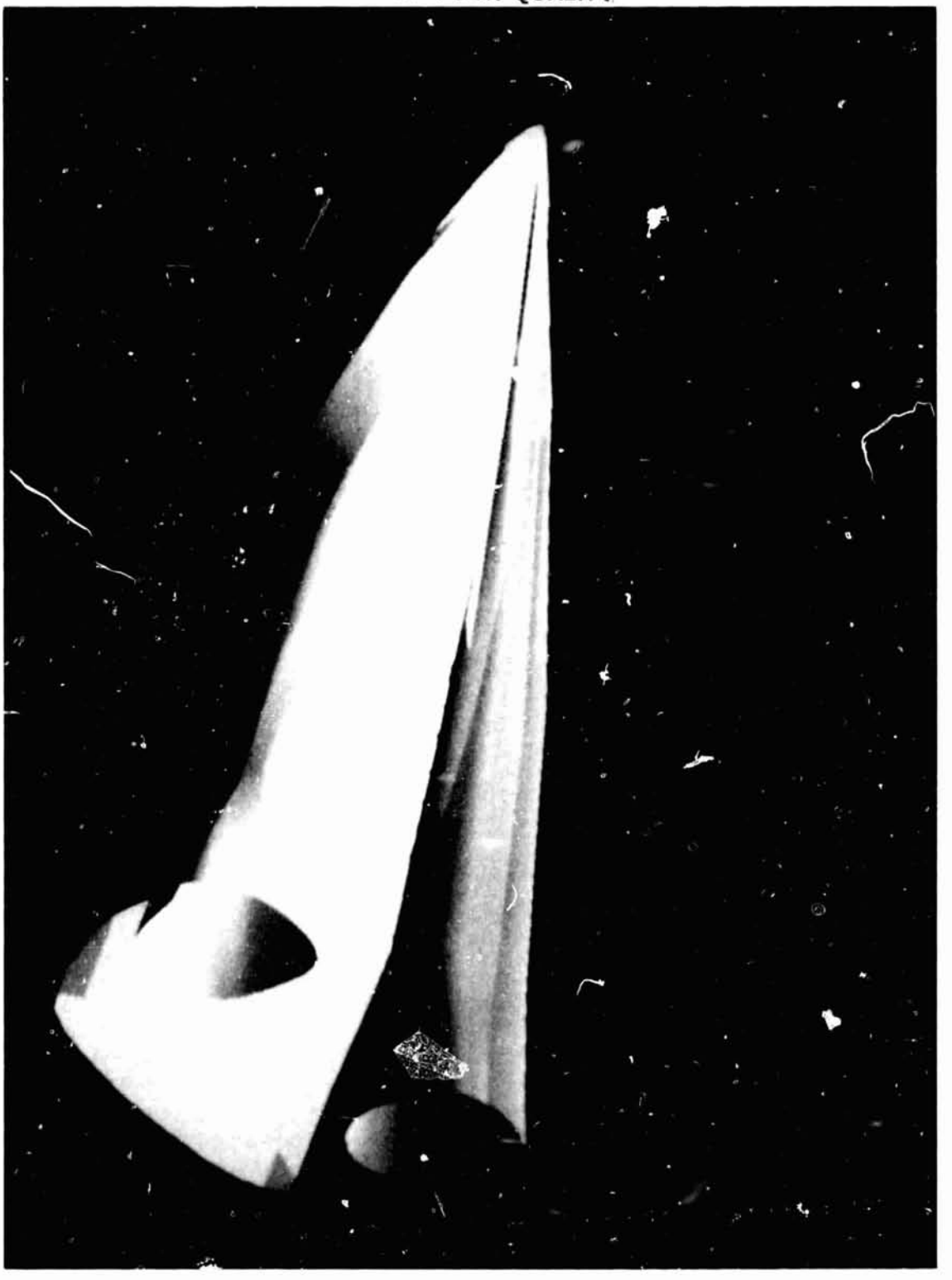

L-85-102

Figure 20.- Example of a computer-generated drawing of vortices produced by an elliptical body.

1. Report No.	2. Government Accession No.	3. Recipient's Catalog No.
NASA TM-86384		

4. Title and Subtitle	5. Report Date
Vapor-Screen Technique for Flow Visualization in the Langley Unitary Plan Wind Tunnel	July 1985
	6. Performing Organization Code: 505-43-23-02

7. Author(s)	8. Performing Organization Report No.
Odell A. Morris, William A. Corlett, Donald L. Wassum, and C. Donald Babb	L-15902
	10. Work Unit No.

9. Performing Organization Name and Address	11. Contract or Grant No.
NASA Langley Research Center Hampton, VA 23665	
	13. Type of Report and Period Covered: Technical Memorandum

12. Sponsoring Agency Name and Address	14. Sponsoring Agency Code
National Aeronautics and Space Administration Washington, DC 20546	

15. Supplementary Notes

16. Abstract

The vapor-screen technique for flow visualization, as developed for the Langley Unitary Plan Wind Tunnel, is described with evaluations of light sources and photographic equipment. Test parameters including dew point, pressure, and temperature were varied to determine optimum conditions for obtaining high-quality vapor-screen photographs. The investigation was conducted in the supersonic speed range for Mach numbers from 1.47 to 4.63 at model angles of attack up to 35°. Vapor-screen photographs illustrating various flow patterns are presented for several missile and aircraft configurations. Examples of vapor-screen results that have contributed to the understanding of complex flow fields and provided a basis for the development of theoretical codes are presented with reference to other research.

17. Key Words (Suggested by Author(s))	18. Distribution Statement
Vapor-screen technique Flow visualization Vapor-screen photographs	Unclassified - Unlimited Subject Category 02

19. Security Classif. (of this report)	20. Security Classif. (of this page)	21. No. of Pages	22. Price
Unclassified	Unclassified	39	A03

For sale by the National Technical Information Service, Springfield, Virginia 22161